

**POLITECNICO DI TORINO**

Dipartimento di Energetica

Corso di Laurea Magistrale in Ingegneria Energetica e Nucleare

Tesi di Laurea Magistrale

**CFD model for tubular SOFC cell fed directly by biomass – complete  
integrated system**



Relatore:

Prof. Massimo Santarelli

Correlatori:

Davide Papurello

Domenico Ferrero

Candidato:

Davide Canuto

**ANNO ACCADEMICO 2018 / 2019**



## Abstract

The DB-SOFC project, in which this thesis is involved, is based on an innovative solution to produce electrical power gasifying, inside the stack, the residual biomass derived from the pruning of the grapevines and olive trees and the production waste of the olive oil that has been properly pre-treated; in particular in this thesis it has been analyzed the last type of biomass for which has been made some studies by UoWM in collaboration with TUC.

The project derives from the necessity to cover the increasing need of electrical power avoiding the usage of non-renewable sources and to make it with unused, or badly used, sources that are present in the Mediterranean area. For this purpose, in the thesis has been conducted many simulation on the tubular cells of two configurations of stack to evaluate if the power that could be extracted from them is higher than the prefixed goal of the project of 200 W. In this work, the fuel that powers the cells has supposed to be only syngas, derived by two different pre-treated biomass (OK500 and OK800) studied by UoWM and TUC, without solid charcoal in contact with the lower part of the cell (instead, the real configuration should be this), supposing three different linear temperature distribution of it between the inlet of biomass and the outlet of syngas. Also two cooling systems has been analyzed to select the best solution to extract more power: the fluid selected for the analysis are liquid water in pressure and air.

From the simulations has emerged that the cooling system that permits to avoid high reduction of temperature near the contact zone between the cell and the cooling system is the one with air. Instead, comparing the two types of biomass, simulated with air as cooling fluid, results that the best performance is obtained with the squared stack with biomass OK500 because it provides 6 W more than the correlative system powered by syngas derived by the gasification of biomass OK800: all the two results are obtained with a linear temperature distribution between 800 °C and 750°C. The other two types of distribution don't permit to satisfy the target of 200 W in every configuration. Moreover, it results the circular stacks are always worse than the squared stacks due to the managing of the current collection.

# Index

<b>1</b>	<b>DB-SOFC project</b>	<b>13</b>
1.1	General overview of the project	13
1.2	Aim of the thesis	15
<b>2</b>	<b>Theoretical background</b>	<b>16</b>
2.1	Fuel cell: generic features	16
2.1.1	Evaluation of the Open Circuit Voltage	19
2.1.2	Overvoltages	21
2.1.2.1	Activation overvoltage	21
2.1.2.2	Ohmic overvoltage	22
2.1.2.3	Diffusion overvoltage	22
2.1.3	Polarization curve	24
2.1.4	Heat generation	25
2.1.5	Efficiency	25
2.1.6	Fuel and Air Utilization	25
2.2	Solid Oxide Fuel Cell description	26
2.2.1	Fuel adaptability	26
2.2.1.1	Carbon deposition	27
2.2.2	Influence of temperature on the cell voltage	28
2.2.3	Different configuration: planar and tubular	28
2.2.3.1	Planar configuration	28
2.2.3.2	Tubular configuration	29
2.3	Biomass and pyro-gasification	30
2.3.1	Pyro-gasification process	31
2.3.1.1	Pre-heating and drying	31
2.3.1.2	Pyrolysis	31
2.3.1.3	Gasification	31
2.3.2	Tars and contaminants	32
2.4	Syngas composition from the gasification	33
<b>3</b>	<b>Studied tubular geometry and material properties</b>	<b>35</b>
3.1	SOFC tubular cell in our project: geometrical description	35

3.2	Stack description	38
4	Modelization	40
4.1	Electrochemical model	41
4.2	Steam methane reforming and water gas shift reactions	45
4.3	Heat management	48
5	Results	52
5.1	2D model validation	52
5.2	Reconstruction of the 2D cell with a length of 16 cm	57
5.3	Development of the 3D model	59
5.3.1	Performance of the 3D cell with water heat removal system	59
5.3.2	Performance of the 3D cell with air heat removal system	65
5.3.3	Comparison between the two cooling systems	67
5.4	3D stacks: power and temperature distribution	69
5.4.1	Squared stack	69
5.4.1.1	OK800: water and air cooling system	69
5.4.1.2	OK500: air cooling system	72
5.4.2	Circular stack	75
5.4.2.1	OK800 circular: water and air cooling system	75
5.4.2.2	OK500 circular: air cooling system	77
6	Conclusions	78
7	Bibliography	80

## Figure index

<b>Figure 1.</b> Production of olive oil in the World	14
<b>Figure 2.</b> Three Phase Boundary; in this figure it is shown only the anodic TPB	17
<b>Figure 3.</b> Schematic representation of a Solid Oxide Fuel Cell	18
<b>Figure 4.</b> Polarization curve of a generic fuel cell	24
<b>Figure 5.</b> Two planar SOFCs connected in series with the interconnectors	29
<b>Figure 6.</b> Biomass composition in terms of main constituent elements	30
<b>Figure 7.</b> Graphs provided by UoWM and TUC that shows the volumetric percentage of the composition of the dry syngas derived by the gasification of the biomass	33
<b>Figure 8.</b> Cathodic air injection design	36
<b>Figure 9.</b> Squared stack geometry (on the left) and circular stack geometry (on the right, a quarter of it)	38
<b>Figure 10.</b> Vertical section of the DB-SOFC stack	39
<b>Figure 11.</b> 2D cross-sectional view of the cell with length of 11 cm	52
<b>Figure 12.</b> Polarization curves of the 2D model with the approximation of the electrodes	Errore. Il segnalibro non è definito.
<b>Figure 13.</b> Power density vs. current density curve of the 2D cell	Errore. Il segnalibro non è definito.
<b>Figure 14.</b> Polarization curve of the 2D model built with volumetric electrodes	Errore. Il segnalibro non è definito.
<b>Figure 15.</b> Power density curve of the 2D model built with volumetric electrodes	Errore. Il segnalibro non è definito.
<b>Figure 16.</b> Polarization curve of a single 16 cm cell	Errore. Il segnalibro non è definito.
<b>Figure 17.</b> Power density curve of a single 16 cm cell	Errore. Il segnalibro non è definito.
<b>Figure 18.</b> Velocity profiles of syngas and air in the 3D cell cooled by water (the right legend is the one for the syngas)	60
<b>Figure 19.</b> Temperature gradients inside the cell and the flow channels with respect to 800 °C, adopting the water heat removal system	61
<b>Figure 20.</b> Molar fraction distribution of H <sub>2</sub>	62
<b>Figure 21.</b> Molar fraction distribution of H <sub>2</sub> O	63
<b>Figure 22.</b> Distribution of chemical species in the anode channel: CH <sub>4</sub> (top left), CO (top right) and CO <sub>2</sub> (bottom)	64
<b>Figure 23.</b> Cathode chemical species distribution: O <sub>2</sub> on the left and N <sub>2</sub> on the right	65

<b>Figure 24.</b> Temperature gradients inside the cell and in the flow channels with respect to 800 °C, adopting the air cooling system	66
<b>Figure 25.</b> Distribution of the molar fraction of H <sub>2</sub> (left) and H <sub>2</sub> O (right)	67
<b>Figure 26.</b> Average temperatures for the two different cooling system	67
<b>Figure 27.</b> Maximum and minimum temperatures for the two different cooling system	Errore. Il segnalibro non è definito.
<b>Figure 28.</b> Electrical power developed by every cell in the three temperature distribution with water cooling system	70
<b>Figure 29.</b> Electrical power developed by every cell in the three temperature distribution with air cooling system	71
<b>Figure 30.</b> Trend of the average temperatures of syngas OK800 for the two cooling system	72
<b>Figure 31.</b> Power distribution inside the squared stack of a row of cells alimented by syngas derived by the gasification of the biomass OK500	74
<b>Figure 32.</b> Distribution of power provided by the cell in every position inside the stack cooled by water and powered by OK 800	75
<b>Figure 33.</b> Distribution of power provided by cells in every position inside the stack cooled by air and powered by OK 800	76
<b>Figure 34.</b> Power distribution inside the circular stack of a row of cells alimented by syngas derived by the gasification of the biomass OK500	77

## Table index

<b>Table 1.</b> Volumetric percentage of each species in the dry syngas	<b>34</b>
<b>Table 2.</b> Volumetric percentage of species contained in the humid syngas	<b>34</b>
<b>Table 3.</b> Material properties of the electrodes	<b>37</b>
<b>Table 4.</b> Material properties of the electrolyte	<b>37</b>
<b>Table 5.</b> Values adopted for the evaluation of the equilibrium current densities	<b>42</b>
<b>Table 6.</b> Values of $\epsilon_i/kb$ and $\sigma_i$ found on literature	<b>44</b>
<b>Table 7.</b> Entropies at temperature of 1073 K	<b>49</b>
<b>Table 8.</b> Thermal parameters of every layer composing the cell [16]	<b>50</b>
<b>Table 9.</b> Temperature distribution of the syngas OK800 and relative species quantities between 800 °C and 750 °C	<b>69</b>
<b>Table 10.</b> Temperature distribution of the syngas OK800 and relative species quantities between 800 °C and 700 °C	<b>69</b>
<b>Table 11.</b> Temperature distribution of the syngas OK800 and relative species quantities between 800 °C and 650 °C	<b>69</b>
<b>Table 12.</b> Effective distribution inside the stack powered by biomass OK800	<b>72</b>
<b>Table 13.</b> Temperature distribution of the syngas OK500 and relative species quantities between 800 °C and 750 °C	<b>73</b>
<b>Table 14.</b> Temperature distribution of the syngas OK500 and relative species quantities between 800 °C and 700 °C	<b>73</b>
<b>Table 15.</b> Temperature distribution of the syngas OK500 and relative species quantities between 800 °C and 650 °C	<b>73</b>
<b>Table 16.</b> Effective distribution for the stack powered by biomass OK500	<b>74</b>

## Acronyms

<b>DB-SOFC</b>	Direct conversion of Biomass to electricity via an internal catalytic gasification Solid Oxide Fuel Cell
<b>GDL</b>	Gas Diffusion Layer
<b>TPB</b>	Three Phase Boundary
<b>SOFC</b>	Solid Oxide Fuel Cell
<b>PEMFC</b>	Proton Exchange Membrane Fuel Cell
<b>YSZ</b>	Ytria Stabilized Zirconia
<b>SMR</b>	Steam Methane Reforming
<b>WGS</b>	Water Gas Shift

## Nomenclature

$A_{i,an/cat}$	Pre-exponential factor [ $S/m^2$ ]
$AU$	Air utilization [-]
$C$	Molar concentration [ $mol/m^3$ ]
$c_p$	Gas specific heat capacity [ $J/(kgK)$ ]
$d_{pore}$	Diameter of electrodes pore [m]
$D^{eff}$	Effective diffusion coefficient [ $m^2/s$ ]
$D_i^{F,K}$	Sum of Fick and Knudsen diffusion coefficient [ $m^2/s$ ]
$D_i^K$	Knudsen diffusion coefficient of a generic species $i$ [ $m^2/s$ ]
$D_{ij}$	Binary diffusion coefficient [ $m^2/s$ ]
$E$	Equilibrium potential [V]

$E_{act,an/cat}$	Activation Energy [J/mol]
$F$	Faraday's constant [C/mol]
$FU$	Fuel utilization [-]
$\bar{g}$	Molar Gibbs free energy [J/mol]
$H$	Heat of reaction [J/mol]
$\bar{h}$	Molar enthalpy [J/mol]
$I_c$	Cell current [A]
$i$	Current density [A/cm <sup>2</sup> ]
$i_{0, an/cat}$	Equilibrium current density [A/cm <sup>2</sup> ]
$i_l$	Limiting current density [A/cm <sup>2</sup> ]
$\bar{l}$	Molar work [J/mol]
$K_{pr}$	SMR Equilibrium constant [Pa]
$K_{ps}$	WGS Equilibrium constant [-]
$k$	Thermal conductivity [W/(m*K)]
$k_{r,forward/backward}$	SMR catalysed reaction rate constant [-]
$k_{s,forward/backward}$	WGS catalysed reaction rate constant [-]
$LHV$	Low Heating Value [kJ/mol]
$M_i$	Molar mass [kg/mol]
$\dot{n}$	Molar flow [mol/s]
$n_{rds}$	Electrons exchanged in the rate determining step [-]
$OCV$	Nernstian voltage [V]
$p$	Pressure [Pa]
$p_0$	Ambient pressure [Pa]
$Q$	Thermal source/sink [W/m <sup>3</sup> ]
$q$	Conductive heat flux [W/m <sup>2</sup> ]
$R_{r/s}$	Volumetric rate of reaction [mol/(m <sup>3</sup> s)]
$r$	Specific resistance [ $\Omega$ *cm <sup>2</sup> ]
$\bar{R}$	Universal gas constant [J/molK]
$\bar{s}$	Molar entropy [J/molK]
$T$	Temperature [K]
$u$	Velocity vector [m/s]
$u_{ion}$	Ionic mobility [m <sup>2</sup> /sV]

$V_c$	Cell voltage [V]
$W_{el}$	Electrical Power [W]
$x_i$	Molar fraction [-]
$z$	Charge number [-]

## Greek symbols

$\beta$	Simmetry factor [-]
$\delta$	thickness of diffusion [m]
$\varepsilon$	Porosity [-]
$\Sigma_{irr}$	Entropy generated by irreversibilities [W/K]
$\eta_{act}$	Activation overvoltage [V]
$\eta_{diff}$	Diffusion overvoltage [V]
$\eta_{el}$	Total electrical efficiency [-]
$\eta_{ohm}$	Ohmic overvoltage [V]
$\lambda_{path}$	Mean free path [m <sup>2</sup> ]
$\nu$	Stoichiometric coefficient [-]
$\rho$	Gas Density [kg/m <sup>3</sup> ]
$\sigma_i$	mean characteristic length of species i [Å]
$\sigma_{ion}$	Ionic conductivity [S/m]
$\tau$	Tortuosity [-]
$\Phi_{th}$	Thermal flux [W]
$\Omega_D$	Dimensionless diffusion collision [-]



# 1 DB-SOFC project

## 1.1 General overview of the project

The project, in which Politecnico di Torino is involved, is the direct conversion of biomass to electricity via an internal catalytic gasification solid oxide fuel cell (called DB-SOFC later).

The work is developed with the universities of the Mediterranean region listed below:

- Technical University of Crete (TUC)
- University of Western Macedonia (UoWM)
- Yildiz Technical University (YTU)
- Karlsruhe Institute of Technology (KIT)
- Mohammed VI Polytechnic University (UM6P)

Moreover, a company named “Mills of Crete” located in the island of Crete, who provides its experience in the field of olive kernel utilization and it will use this technology to innovate the process of the corporation.

Also the INCAR-CSIC, a researching spanish carbon institute, that takes part to the project with studies on the biomass source.

The goal of this project is to generate electrical current from a stack of tubular cell fed continuously by biomass that can be available in the country of the Mediterranean Region, in particular the biomass, that will be studied, is olive kernel, olive pomace and pruning of the grapevines and of the olive trees.

The project arises to overcome the necessity to exploit the organic residual by the agricultural activity and to utilize them on a less pollutant and more efficient way than the traditional one.

An efficient way to reach this goal could be the one adopted in this work, that is to use a stack of SOFC tubular cells connected in series and in parallel to generate current: a SOFC is an electrochemical device that can provide electrical power from the reactions of the fuel and the oxidant that are send, respectively, to the anode and the cathode of the cell with the electrons that circulate between these two electrodes through a wire connection. The reactions are possible due to the transport of  $O^{2-}$  ions in the electrolyte placed in the middle of the two electrodes.

The fuel is derived by the innovative part of this project: the gasification directly inside the stack.

The gasification is a process in which there is the conversion of a solid/liquid organic compound (the charcoal/biofuel derived by the pyrolysis process) on a gas/vapour phase (called syngas) and a solid phase (ashes) [1] and the operation temperature of this practice is almost 900 °C. The syngas is the product that has a useable heating value and the dominant reaction that occurs in this process is a partial oxidation done with oxygen, air, steam or CO<sub>2</sub>, (or a combination of them). In our case the oxidants are H<sub>2</sub>O and CO<sub>2</sub>.

The biomass, as we told before, that it's used for this project is the olive kernel, olive pomace and the residues of pruning of olives trees and grape vines because they are the primary sources of biomass in the Mediterranean Region because Italy, Spain, Greece, Turkey and Morocco hold more than 85% of the world's olive production and they cultivate, at the same time, large areas with grape vines[2] For example, in Morocco, as reported by Alami and El Achaby[3], are produced 1.500.000 tons of olives from which all farms obtain 160.000 tons of olive oil and 90.000 tons of table olives (data referred to January 2018). Therefore, this production generates a large amount of organic residual because, according to the report of Alami and El Achaby, to produce 1 liter of olive oil are needed about 4 to 8 kilos of olives with an average production of 5 kilos of olive pomace, the olive pits are estimated to be the 10 % of the olives fruit used for oil extraction and the olive pruning produced is almost 3 tons/hectare per year.

Morocco contributes in small part at the world production of olive oil (it is part of the 32.39% in the Figure 1) which amounts at 3.2 million of tons<sup>1</sup> and it was the fifth largest producer of olives worldwide in 2012.

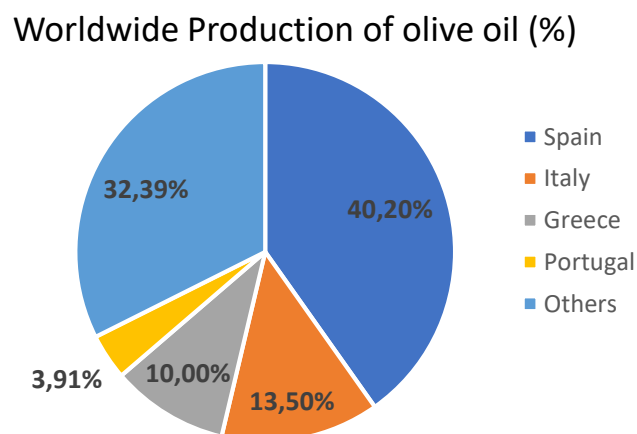


Figure 1. Production of olive oil in the World

<sup>1</sup> Link: <https://itsagroalimentareveneto.it/lavanzata-dellolio-di-oliva/>

Instead, in Greece there is a production of almost 2.200.000 tons of olives only for the olive oil production, at which we have to add the production of table olives[4] .

Regarding to the vineyards, the area cultivated to produce grapes in Morocco is 49 000 hectares (data referred to season 2015/2016) and the total amount of grape vine pruning residue can be estimated to 1.2-3.5 tons/hectare[5]. Also in this case Morocco is below the other countries that work to this activity in the worldwide ranking of wine producer[3], so we can affirm that the amount of biomass produced by each nations is higher than the production of Morocco.

## **1.2 Aim of the thesis**

The goal of this thesis is to create a 3D-simulation on Comsol Multiphysics® of a stack of SOFC tubular cells able to generate 200 W of electrical power, this work starts from the considerations done by my colleague Valentina Somano in her previous work of 2D-simulation of the same cell.

It will be compared two different configurations to decide which is the best in terms of current density developed and thermal distribution. For this purpose, it has been selected two main configuration:

1. Modellization of a square stack with a 32 cm side
2. Modellization of a circular stack with a diameter of 36,28 cm

The fuel that will provide the chemical energy is a syngas, with the composition evaluated by the UoWM in collaboration with TUC, derived by the gasification process, and it will be used on a hypothetical fuel channel that will be modelled around every cell surface.

At the end of the thesis it will be possible to compare the two configurations proposed and select the one with the best performance.

In the future will be developed works that simulate the two configuration taking into account the complete gassification process inside the stack to make as real as possible the simulation. The results obtained by these simulations, if the project is feasible, will be compared with experimental tests done in laboratory on the prototype that will be developed by the Karlsruhe Institut of Technology in its laboratory.

## 2 Theoretical background

### 2.1 Fuel cell: generic features

One of the methods to avoid the combustion process to generate current is the use of a fuel cell which is a direct method of production and it guarantee an higher efficiency than the combustion process.

The fuel cell is an electrochemical device composed by two porous electrodes (one anode and one cathode) and an electrolyte in between of them, in which there is a conduction of anion, or cation, depending on the type of the machine. Then, the cells are connected to form a stack with the presence of the interconnectors that give to the stack the robustness and they are shaped to create a channel flow to guarantee the flow of the reactants towards the electrodes.

It's possible to collect the current only with the presence of an external electrical circuit, therefore also the electrodes must be able to conduct current. So, the constituent material is usually an high conductive material.

Every electrode is composed by two layers:

- one is the so called Gas Diffusion layer (GDL) that is the electrode without the catalyst and in which don't occur the reactions. This layer is often composed by carbon fibers that is a porous material and it has the function of providing an electrically conductive pathway for current collection. Furthermore, the principal functions of this layer are: guarantee the gas diffusion from the flow channel to the layer described at the following point, remove the heat produced during cell operation, remove the water produced and the surplus reactants and protect the other layer from corrosion or erosion induced by flows or carbon deposition
- the other one is the catalyst layer and on it, as we can deduce from its name, is deposited by a deposition process the catalyst useful for the specific reaction that will be catalyzed on it.

In the catalyst layer the reactions take place and, around a grain of catalyst, three phase coexist:

- The porous phase in which pass through the fuel/oxidant
- The electronic phase, where the electrons produced (or utilized) are removed (or led)
- The ionic phase, path followed by the ions conducted in the electrolyte

This locus is called the Three Phase Boundary (TPB) and it is located near the boundary that divides the electrode from the electrolyte. As it can be seen in the Figure 2, i.e for the anodic side of a Solid Oxide Fuel Cell (SOFC), the hydrogen (that in this case is the fuel) goes in contact with the Nickel

catalyst and reacts with  $O^{2-}$  ions transported by the electrolyte releasing the electrons, that will be transported by the Nickel, and the produced water.

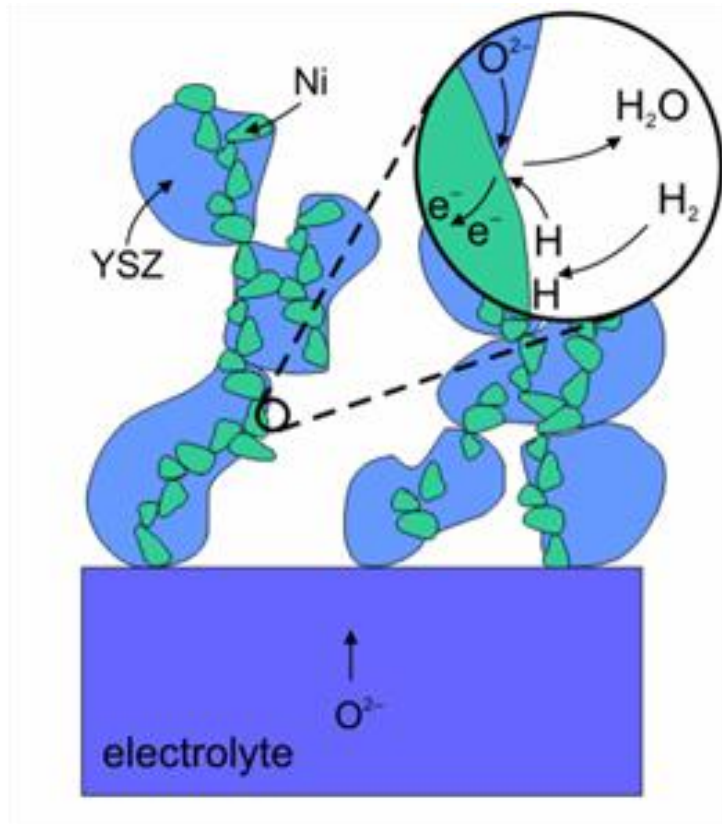


Figure 2. Three Phase Boundary; in this figure it is shown only the anodic TPB

For what concern the electrolyte, the material depends on the type and, thus, the temperature of the fuel cell: if the cell is a PEMFC (low temperature cell), the most common material is the NAFION. Contrariwise, the Yttria-Stabilized Zirconia (YSZ with 8% of  $Y_2O_3$ ) is the most used constituent in SOFC application.

The electrolyte must be able to conduct the ions but it has to avoid the electronic and molecular conduction for reducing, as much as possible, the cross-over effect: harmful effect that consists in the involuntary passage of fuel, or oxidant, through the electrolyte. This effect is not completely avoided because the electrolyte diffusion coefficient of molecules and electrons conductivity are not zero, so a little quantity of molecules pass through it. Cross-over effect is influenced by the thickness of the electrolyte because if it increases, the cross-over effect will decrease, but the Joule effect increases and it generates a voltage drop.

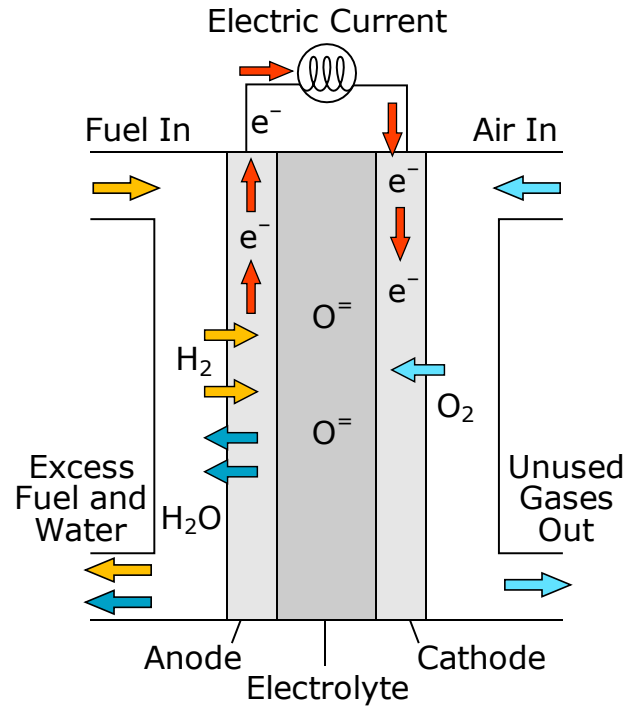


Figure 3. Schematic representation of a Solid Oxide Fuel Cell

The conduction of ions in the electrolyte permits to produce a voltage drop after a reaction of oxidation of the fuel (usually  $H_2$  or a carbonaceous one) at the anode, negative pole of the cell, that provides electrons which they will be used in the reaction of reduction that occurs at the cathode, positive pole of the cell, when the circuit between the two electrodes will be closed, so it's obtained an electrical current.

To asses the conductivity of the ions in the electrolyte the formula is:

$$\sigma_{ion,i} = z_i^2 * F^2 * C_i * u_{ion,i} \quad (1)$$

where

- $z_i$  is the charge number
- $F=96485$  [C/mol] is the Faraday's constant
- $C_i$  is the concentration of the ion in the electrolyte material in [mol/m<sup>3</sup>]
- $u_{ion,i}$  is the ionic mobility in [m<sup>2</sup>/s\*V]

Instead, the current developed by the fuel cell can be evaluated with the Faraday's Law:

$$I_c = z_i * F * \dot{n}_i \quad (2)$$

where

- $F=96485$  [C/mol] is the Faraday's constant
- $z_i$  is the charge number
- $\dot{n}_i$  is the molar flow of reactants or products of the reaction in [mol/s]

So, it's possible to calculate the power produced as:

$$W_{el} = I_c * V_c \quad (3)$$

$V_c$  represents the voltage developed by the cell under operating condition and it can be assessed with the expression:

$$V_c = OCV - \eta_{act} - \eta_{ohm} - \eta_{diff} \quad (4)$$

The terms are, respectively, the Open Circuit Voltage, difference of potential between the two electrodes when there isn't flow of electrons in the electrical circuit( condition called "Open Circuit"), the activation overvoltages that represent the losses due to the activation of the electrochemical reactions at the anode and at the cathode, the ohmic overvoltage that involves the losses due to the charge conduction both in electrodes (conduction of  $e^-$ ) and in the electrolyte (conduction of ions) and the diffusion overvoltages corresponding to the losses that arise in the electrodes as a consequence of a difference of molar concentration of reactants between the anodic, or cathodic, active layer and the support layer of the same electrode.

The discussion of each of them will be elaborated on the next paragraphs.

### 2.1.1 Evaluation of the Open Circuit Voltage

The open circuit voltage (OCV) can be evaluated applying the first and second law of the thermodynamic to the fuel cell in open circuit condition

$$\left\{ \begin{array}{l} \Phi_{th} - W_{el} = \sum_i^{products} \dot{n}_P * \bar{h}_P(T, p_i) - \sum_i^{reactants} \dot{n}_R * \bar{h}_R(T, p_i) = \Delta \bar{h}_{reaction} \\ \frac{\Phi_{th}}{T} + \Sigma_{irr} = \sum_i^{products} \dot{n}_P * \bar{s}_P(T, p_i) - \sum_i^{reactants} \dot{n}_R * \bar{s}_R(T, p_i) = \Delta \bar{s}_{reaction} \end{array} \right. \quad (5)$$

and normalizing both with respect to  $\dot{n}_{fuel}$ , which is the chemical species oxidised at the anode, and then combining the two laws making the hypothesis of negligible irreversibilities because the transport phenomena in open circuit is negligible.

So, I can obtain the molar electrical work:

$$\bar{l}_{el} = -\Delta \bar{h}_{reaction} + T * \Delta \bar{s}_{reaction} = -\Delta \bar{g}_{reaction} \quad (6)$$

Then, I have to asses the same quantity with another method to achieve the OCV.

$$\bar{l}_{el} = \frac{W_{el}}{\dot{n}_{fuel}} = \frac{I_c * OCV}{\frac{I_c}{z_{fuel} * F}} = z_{fuel} * F * OCV \quad (7)$$

At the end, comparing equation (6) and (7), I can conclude

$$OCV = -\frac{\Delta \bar{g}_{reaction}}{z_{fuel} * F} \quad (8)$$

This is the Nernst Equation for the fuel cells that are devices with a negative  $\Delta \bar{g}_{reaction}$ .

If I put in evidence the dependency of the Gibbs free energy on the partial pressure of reactants and products, the Nernst equation becomes this:

$$OCV = -\frac{\Delta \bar{g}_{reaction}(T, p_0)}{z_{fuel} * F} + \frac{\bar{R} * T}{z_{fuel} * F} * \ln \left( \frac{\prod_1^n \left(\frac{p_i}{p_0}\right)^{\nu_i}}{\prod_1^m \left(\frac{p_i}{p_0}\right)^{\nu_i}} \right) \quad (9)$$

where:

- $\bar{R} = 8.314$  [J/molK] is the Universal gas constant
- $n$  and  $m$  represent, respectively, the number of reactants and products involved in the reactions
- $p_0 = 1$  [bar], is the ambient pressure
- $\nu$  is the stoichiometric coefficient of each species

Therefore, it is possible to conclude that the OCV depends only on the thermodynamics and it isn't based on variation of the current inside the cell.

## 2.1.2 Overvoltages

The cell will provide energy only if the equilibrium will be broken, this means that the external circuit will be closed, but under operating condition the cell undergoes a reduction of the voltage due to the beginning of the transport phenomena that produce overvoltages, so there is a reduction of the equilibrium voltage when the current inside the cell increase because all these quantities, as shown in the next paragraphs, directly depends on current.

### 2.1.2.1 Activation overvoltage

This first type of reduction is caused by an energy that has to be spend to activate the electrochemical reactions at the cathode and at the anode to increase the rate of reactions. The overvoltage can be evaluated applying the Butler-Volmer equation to the two electrodes

$$i = i_0 * \left\{ \exp \left[ \frac{\beta * n_{rds} * z * F}{\bar{R} * T} * \eta_{act} \right] - \exp \left[ \frac{-(1 - \beta) * n_{rds} * z * F}{\bar{R} * T} * \eta_{act} \right] \right\} \quad (10)$$

where:

- $\beta$  is the simmetry factor, that represent a ratio of the activation energy
- $n_{rds}$  is the number of electrons exchanged in the rate-determining step

- $i_0$  is the current density developed when the electro-chemical reaction is in equilibrium (open circuit condition)

and to obtain the value of  $\eta_{act}$ , but it isn't so trivial because  $\beta$  isn't known. However, from experimental results, this value can be assumed equal to 0.5[6].

Now, the expression of  $\eta_{act}$  could be found:

$$\eta_{act} = \frac{\bar{R} * T}{\beta * n_{rds} * z * F} * \sinh^{-1} \left( \frac{i}{2 * i_0} \right) \quad (11)$$

As mentioned before, the Butler-Volmer equation must be applied to each electrode, so in the eq. (4) the activation overvoltage are two: one anodic and one cathodic.

### 2.1.2.2 Ohmic overvoltage

This type of loss is due to the ions and electrons transport phenomena in the fuel cell and it can be expressed with the Ohm's law:

$$\eta_{ohm} = r * i = (r_{el} + r_{ion}) * i \quad (12)$$

in which the  $r$  is the specific resistance in  $\Omega \cdot \text{cm}^2$ .

### 2.1.2.3 Diffusion overvoltage

The last loss that decrease the voltage of a fuel cell is the one due to the mass transport (diffusion) of the fuel/ oxidant from the support layer to the place where the reaction occurs: the Three Phase Boundary. Also in this case the overvoltage is present both in the anode and in the cathode.

In general, there are three models to describe this phenomenon:

- Fick's Law
- Stefan-Maxwell model

- Dusty Gases model

But, for simplicity, the diffusion is described using the model proposed by Fick.

$$J = D^{eff} * \frac{dC}{dx} \quad (13)$$

and combining it with the Faraday's law it can obtain the current density (14) and, consequently, the limiting current density (15)

$$i = D^{eff} * z * F * \frac{C_{\infty} - C_0}{\delta} \quad (14)$$

$$i_l = z * F * D^{eff} * \frac{C_{\infty}}{\delta} \quad (15)$$

in which  $\delta$  represents the thickness of diffusion of reactants,  $C_{\infty}$  is the concentration of the reactant outside the electrode (bulk flow),  $C_0$  is the concentration on the reaction zone (GDL layer) and  $D_{eff}$  corresponds to the effective diffusion coefficient that depends on the porosity,  $\epsilon$ , and tortuosity,  $\tau$ , of the porous electrode according to the following relation:

$$D^{eff} = D_i^{F,K} * \frac{\epsilon}{\tau} \quad (16)$$

and  $D_i^{F,K}$  is the sum of the Fick and Knudsen diffusion coefficients of the reactant outside the electrode (bulk flow).

Finally, the expression of  $\eta_{diff}$ , that can be found on literature is

$$\eta_{diff} = \frac{\bar{R} * T}{z * F} * \ln \left( \frac{C_0}{C_{\infty}} \right) \quad (17)$$

At the end, dividing the eq. 14 by the eq. 15 and substituting the ratio contained in the logarithm with the value obtained, it results the following equation for the diffusion overvoltage

$$\eta_{diff} = \frac{\bar{R} * T}{z * F} * \ln \left( 1 - \frac{i}{i_l} \right) \quad (18)$$

### 2.1.3 Polarization curve

Combining all the contribution with respect to the Eq. (4), it's possible to obtain the i-V curve that describes the trend of the cell voltage when the current density increase and it is called “Polarization Curve”.

In this curve we can distinguish, as in the figure 4 below, three main zones in which the effect of every overvoltage is predominant. In the first part of the curve (low current density zone) the voltage drop is caused by the energy consumption for the activation of the reactions that occur at the anode and at the cathode, then it can be distinguished a linear zone in which the voltage drop is linearly dependent on the current density, as specified in the paragraph 2.1.2.2. In conclusion, in the last zone the behaviour of the curve is mainly influenced by the transport phenomena (diffusion).

Nevertheless, the polarization curve can be affected by the operating temperature and pressure of the fuel cell, the fuel utilization, the air utilization and the reactants used for the reactions.

Moreover, the current density is linearly dependent on the mass flow rate of the fuel, but this quantity is limited to a minimum value to avoid a possible starvage in the pores of the electrodes.

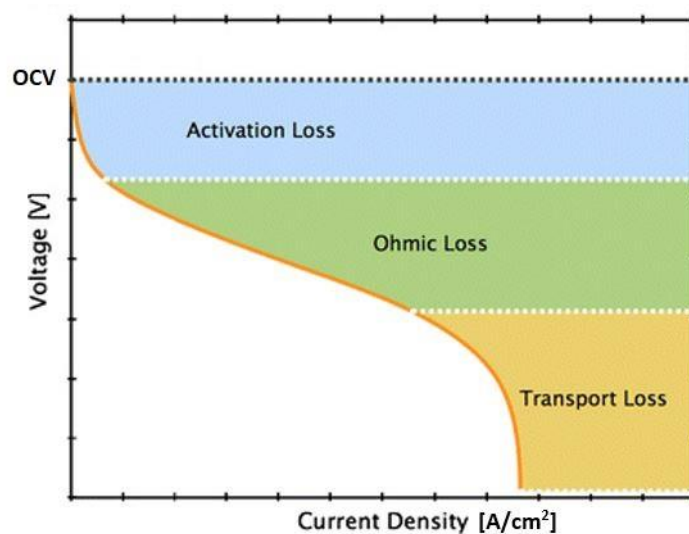


Figure 4. Polarization curve of a generic fuel cell

$$\eta_{el} = \frac{W_{el}}{\dot{n} * LHV_{fuel}} \quad (20)$$

### 2.1.4 Heat generation

Under operating condition, the fuel cell produces also a part of thermal power and it's due to two contribution: the first is a reversible contribution related to the entropy variation in the electrochemical reaction and the other is an irreversible contribution due to the losses described by the overvoltages.

The heat generated can be evaluated with the following formula found in literature:

$$\Phi_{th} = \left( -\frac{\Delta\bar{h}}{z * F} - V_c \right) * I_c \quad (19)$$

### 2.1.5 Efficiency

In conclusion, like as for every energetic device, it can be calculated an overall efficiency that correlates the electrical power,  $W_{el}$ , produced by the fuel cell with the energetic load of the fuel employed to make the reaction inside the anode according to the formula

where  $\dot{n}$  is the molar flow of the fuel and  $LHV_{fuel}$  is its Low Heating Value.

### 2.1.6 Fuel and Air Utilization

Two other important parameters that can be evaluated for a fuel cell are the Fuel and Air Utilization, respectively, indicated as FU and AU. These two parameters represent the deviation from the stoichiometric condition of the quantities of air and fuel injected in the cell to obtain a certain power. Their value will be evaluated by the formulas:

$$FU = \frac{\dot{n}_{fuel,stoich}}{\dot{n}_{fuel,real}} \quad ; \quad AU = \frac{\dot{n}_{air,stoich}}{\dot{n}_{air,real}} \quad (21)$$

## 2.2 Solid Oxide Fuel Cell description

Solid Oxide fuel cells are a subset of the fuel cell's family and they can reach the highest temperature (600 – 1000 °C) among all fuel cell technologies, so they have been chosen for this study to match both the necessity of high temperature for the biomass gasification and the necessity to harness the biomass material with very low pollutant systems.

SOFCs use, as the acronym suggests, a solid ceramic material acting as electrolyte able to conduct oxygen ions from the cathodic side to the anodic electrode. These two electrodes are both composed of a ceramic composite material, but the first one has a Perovskite structure and the other one is a zirconia doped with atoms of metallic Nickel.

The principal advantages presented by this type of cell are:

- High operational temperature, so the transport process are favoured and, in this case, a perfect match is guaranteed with the biomass gasification
- High efficiency, in the range of 50 – 60 %
- Very high fuel adaptability
- Catalyst of lower quality respect to the PEMFC application: SOFC uses the Ni catalyst that permits to have the reforming directly inside the stack
- Work well in stationary condition
- Low NO<sub>x</sub> and SO<sub>x</sub> emissions

And the disadvantages are mainly the slow start-up, shut-down, ramp-up and rump-down, so for this reasons this typology of fuel cell isn't suitable for system with dynamic operations like autovehicles and smart grids. Last, but not least, another drawbacks derived from the utilization of carbonaceous fuels that gives SOFC an high adaptability to fuel consumption, but it can cause the carbon deposition on the electrode in contact with the fuel.

### 2.2.1 Fuel adaptability

As said before, SOFC works with an high variety of carbonaceous fuel (i.e syngas, biogas, carbon monoxide, methanol, etc.) with, obviously, different configuration in terms of balance of plant. The usage of pure hydrogen, as for the PEMFC, is not so convenient because when it reacts with the oxygen ions produces an high quantity of heat that sharply increase the temperature of the stack.

However, from the only electrochemistry point of view, the hydrogen is the fuel that guarantees better performances.

Nevertheless, the better solution is to use, as already said, alternative fuels composed by a mixture of various compounds like as syngas (composed mainly of CO, H<sub>2</sub>, CH<sub>4</sub> and CO<sub>2</sub>) or biogas (mixture of CH<sub>4</sub> and CO<sub>2</sub>) because at the anode, or on a reformer inside the stack, the methane reacts with the water vapour in an endothermic reaction, called Steam Methane Reforming (SMR), that subtracts a part of the heat released by the other reactions that take place in the stack, facilitating the thermal management of the entire stack. In this case it is said that there is an internal reforming. The performance of the cell is still high due to the formation of hydrogen in the SMR ( $CH_4 + H_2O \rightarrow 3H_2 + CO$ ) and in the WGS ( $CO + H_2O \rightarrow H_2 + CO_2$ ).

### 2.2.1.1 Carbon deposition

The usage of carbonaceous fuels, as previously analyzed, is the best solution from the point of view of the balance of plant, but they could deteriorate the performance of the cells producing a deposition of carbon atoms in the TPB of the electrode, inhibiting its normal functioning. This phenomenon, called “Carbon Deposition”, is favoured by the operating temperature of the SOFC and the catalyst (Ni) of the electrode, so the reactions that take place are the methane cracking (Eq. 22) and the Bodouard reaction (Eq. 23)



and they deliver carbon atoms during the SOFC operation and, after a certain period, the pores of the electrode could be obstructed, thus the fuel doesn't able to reach the TPB and the electrochemical reactions can't occur. Moreover, the oxygen ions flux from the electrolyte continues and the oxygen that reaches the anodic side reacts with the atoms of solid Nickel to form NiO, a molecule larger than the Ni, at the interface anode-electrolyte, so it occupies a large volume and it generates stress on the electrode and the electrolyte. The properties of the anodic electrode permit to support the tension generated by this new formed molecules, but the electrolyte undergoes to this stress and there will be a rupture on it. It will generate a degradation of the cell performance and an increase of temperature consequently to an increasing of the conductivity of the oxygen molecules that reach more easily the anode and permit the occurrence of chemical oxidation of the fuel.

## **2.2.2 Influence of temperature on the cell voltage**

The temperature influences the performance of the SOFC: it will reduce the OCV, if it increases, because the molar Gibbs free energy of the reaction depends on it, as in Eq. 9, and the ionic conductivity is sufficiently high only at temperatures in the range of 700-800 °C. Therefore, the nominal voltage of a SOFC is lower than the one of the PEMFC due to the higher temperatures at which the cell must be kept. In this work, the nominal voltage is hypotized to be 0.7 V.

Furthermore, the temperature must be maintained above the value of 700 °C to guarantee that the SMR reaction is pushed towards the products, that will react to provide energy.

## **2.2.3 Different configuration: planar and tubular**

The two principal configuration of this type of cells are represented by the planar and the tubular one.

The cell of the first type is composed by three square, or circular, plate that constitute the two electrodes and the electrolyte, instead, in the tubular cells the three layers have the shape of a tube closed to an extreme. In particular, it can be distinguished one main layer that gives to the device the robustness, so it could have cells electrolyte-supported, anode-supported or cathode supported.

The voltage produced by a single cell in nominal condition is lower than 1 V, so to exploit these elements to produce power is necessary to connect some cells in series, or in parallel, on a stack with interconnectors that are metal elements, appropriately shaped, that put in electrical contact the cathode of one cell with the anode of a nearby cell.

### **2.2.3.1 Planar configuration**

The planar configuration is the simplest of the two, but it has the lowest cost of production[7] and it has sealing problems caused by thermal expansion. The most common methods of production are: dry pressing and screen printing techniques. Moreover, in this type of cell interconnectors have the double function of distributing the gas flows at the correct side and collecting the current developed by the stack. Nowadays, the most promising material for interconnectors is the CROFER 22 APU with a concentration of chromium of 22 %, but it can cause at the cathode the chromium poisoning due to high temperature: it is a process in which the chromium in the interconnectors oxidizes coming into contact with the oxygen flow in the cathodic flow channel. Furthermore, a contact resistance arises between the electrode and the interconnector and the ohmic drop grows, but it can be avoided putting a ceramic paste between them.

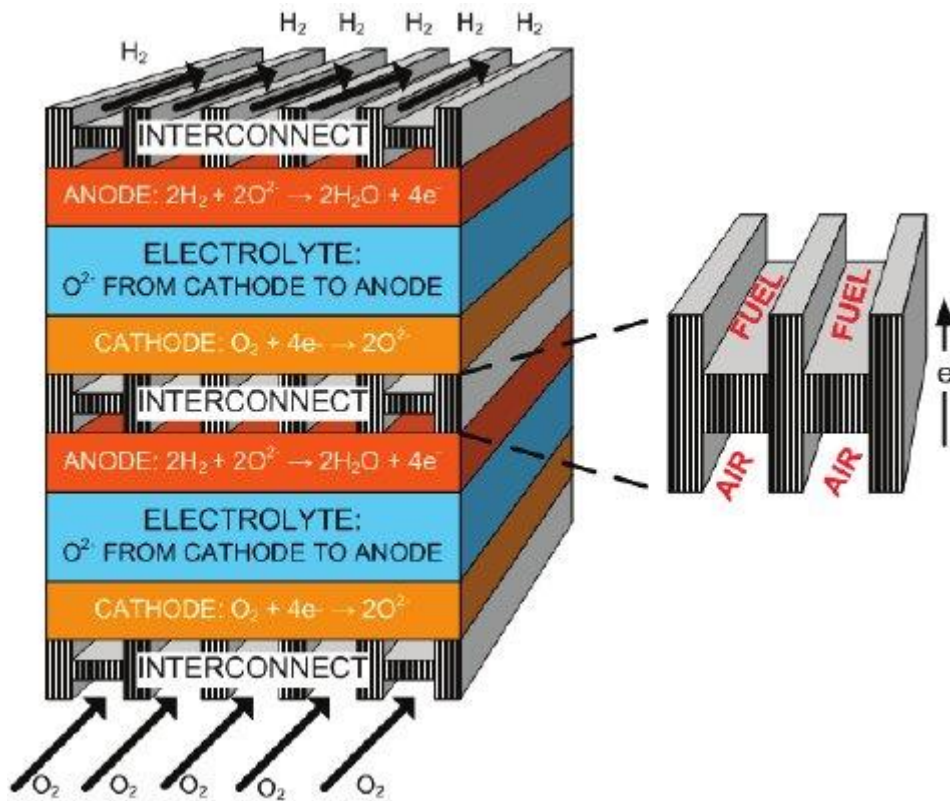


Figure 5. Two planar SOFCs connected in series with the interconnectors

### 2.2.3.2 Tubular configuration

The first tubular configuration has been designed by the US Westinghouse Electric Corporation in the 70s and it was composed by a support tube of calcium stabilized zirconium of thickness of 1-2 mm that worked as structural and functional component because the other layers were deposited on it and it acted as cathode.

Nowadays, the principal material used for the layers are: LSM for the cathode, YSZ for the electrolyte and Ni-YSZ for the anode.

In this configuration the fuel flows on the external surface of the cell and the oxidant agent, often air, flows on a tubular pipe and, initially, is heated up on it and at the end of the internal tube exits and go back to the top of the cell reacting with the electrons and producing the oxygen ions useful to the overall reaction. This happens because the tubular cell is closed to one extreme as in Figure 8 in chapter 3.

## 2.3 Biomass and pyro-gasification

For the project, the most analyzed biomass is the woody biomass derived by the residues of the wine and oil production that, usually, are not used or burned for rural heating. So, our goal is to produce electrical energy that has an higher quality than the thermal one and to make it with an high efficiency.

The lignocellulosic biomass is composed by 3 main parts:

- Cellulose (~ 50 % on dry basis): along chain of organic polymer constituting the fibers
- Hemicellulose (~ 25 % on dry basis): chains of heteropolymers acting as glue for the fibers)
- Lignin (~ 25 % on dry basis): organic polymer it gives robustness and resistance to the degradation

and the biomass constituents are composed mainly by atoms of C, H, N, O, S with a variable part of water and a smaller one represented by the ashes.

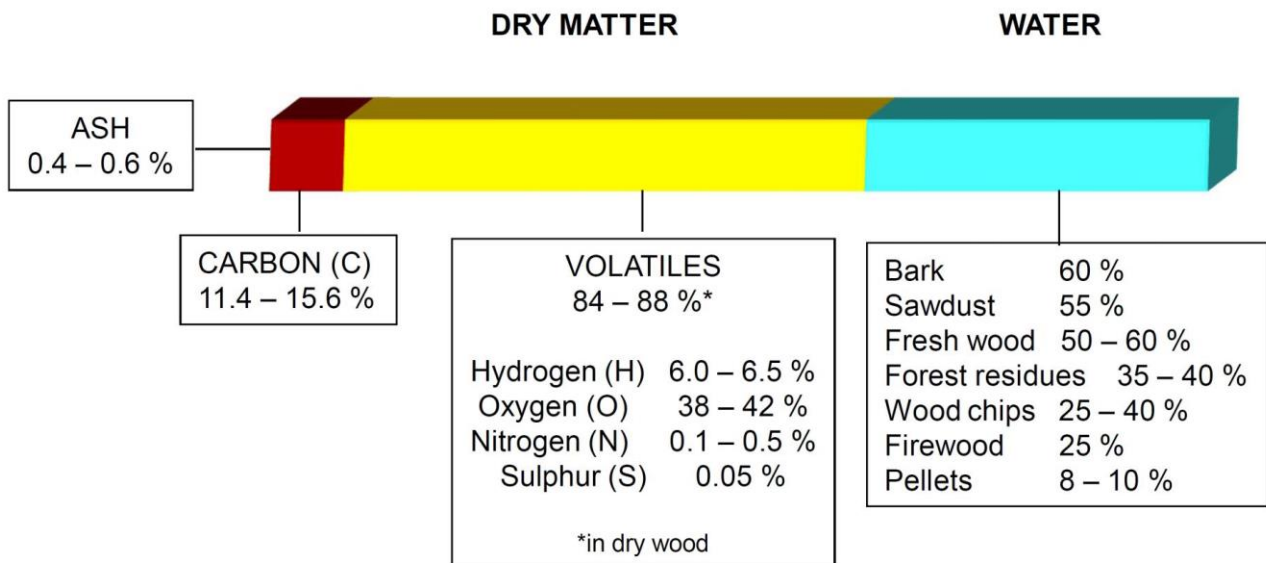


Figure 6. Biomass composition in terms of main constituent elements

Biomass is considered a renewable source if its growing rate is higher than the amount consumed and it has the advantage to be a predictable source.

The main drawbacks due to the harness of this type of material are represented by the fact that the biomass is not abundant, it has an energy and water-intensive production and its growing rate is slow.

### 2.3.1 Pyro-gasification process

Before the utilization, this source must be subjected to a process called “pyro-gasification” in which pre-treated biomass (it can't be used as-received from the harvesting, so it is necessary to mill the organic residues in thinner parts called “pellets”) is transformed in syngas (a mixture of H<sub>2</sub>, H<sub>2</sub>O, CO, CO<sub>2</sub> and CH<sub>4</sub>) by means of a gasifying agent that is usually CO<sub>2</sub>, H<sub>2</sub>O, O<sub>2</sub> or a mixture of them.

The process foresees three steps:

- Pre-heating and drying (<200 °C)
- Pyrolysis (200-600 °C)
- Gasification (600-1000 °C)

#### 2.3.1.1 Pre-heating and drying

Before the gasification, the biomass must be dried to reduce its water content as much as possible to avoid an high energy consumption for the evaporation of the water that amounts to 2500 KJ for 1 kg of H<sub>2</sub>O. Usually, this process is conducted with the use of heat released by the syngas flow exiting from the gasifier reactor at temperature of almost 900-1000°C.

#### 2.3.1.2 Pyrolysis

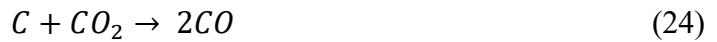
Pyrolysis is a reaction of thermal decomposition conducted in total absence of oxygen that transform the volatile part of biomass in gas compounds (water vapour, methanol, acetic acid) and bio-oil, and the remaining solid part is called “char”.

This process can't be neglected because is longer than in the gasification process of the coal.

#### 2.3.1.3 Gasification

Char produced on pyrolysis step are, then, partially oxidized with a gasifying agent to produce the syngas. Usually, the gasifying agent is air, steam or CO<sub>2</sub> (or a mixture of them).

This part of pyro-gasification process is ulteriorly subdivided in two fundamental reactions: oxidation and reduction. In the first one, the oxygen, injected in under-stoichiometric quantity, reacts with the carbon that constitute the biomass and forms the CO<sub>2</sub> that carries out the inverse Boudouard reaction (Eq. 24) in the reduction zone with the carbon of the biomass. Hereafter, the produced CO of this reaction reacts with the water vapour to form H<sub>2</sub> and CO<sub>2</sub> in the so called Water Gas Shift reaction (WGS) (Eq. 25).



Moreover, in this phase also secondary reactions take place and they are listed below:



### 2.3.2 Tars and contaminants

During the gasification process could be produced organic compounds, called “tars”, with a boiling temperature above that of benzene and their formation is favoured if the temperature in the gasifier is in the range 500-1000°C. Tars are divided in four categories that have an increasing level of damage from the first to the fourth category that corresponds also to an increase of the temperature.

All the reactions in the gasification process, except for the WGS, are favoured by the high temperature and this could allow to crack tars increasing the temperature in the gasifier but it is not so convenient because it requests a large amount of energy to reach this temperature.

Tars, and other contaminants contained in the fresh fuel, as sulfurs, halogens and siloxanes, can cause degradation on the performance of every cell.

## 2.4 Syngas composition from the gasification

As said before, the gasification process produce a gas with variable concentrations of  $H_2$ ,  $CO$ ,  $CO_2$ ,  $CH_4$  and  $H_2O$  with respect to the temperature of pre-treating of the biomass. In particular, the gasification of olive kernel and the grapevines has been studied by the UoWM and TUC and they show their results in the first periodic report of the project.

The results are summarized in the four graphs showed below

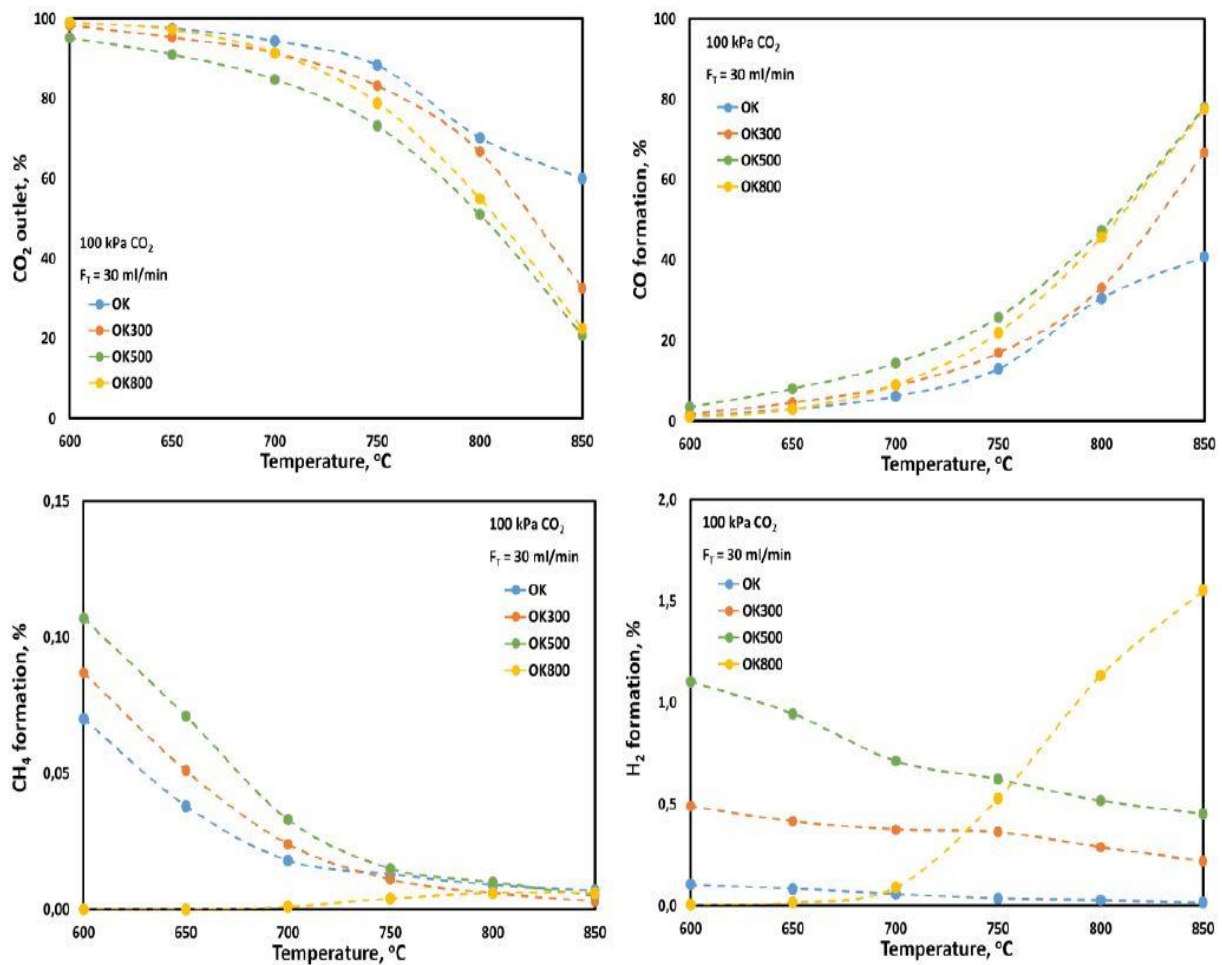


Figure 7. Graphs provided by UoWM and TUC that shows the volumetric percentage of the composition of the dry syngas derived by the gasification of the biomass

and from them it can be extracted the percentage of every species inside the syngas and it is decided to choose the curve OK800, that corresponds to the pre-heating of the biomass at 800 °C, because it generates the highest amount of  $H_2$  at the operative temperature of the cell (results summarized in Table 1) and a similar quantity of the other two reactive molecules. The results represent the

volumetric percentage of species on the dry syngas and the useful values have been assumed at the temperature of the stack, 800 °C.

	$CO_2$	$CO$	$CH_4$	$H_2$
<i>%vol., dry syngas</i>	54	44.8	0.01	1.19

Table 1. Volumetric percentage of each species in the dry syngas

Afterwards, these quantities have been recalculated considering the syngas with its water content that is, according to the thesis of Guizani[8], the 10 %wt of biomass and the ratio will be maintained constant on the syngas produced.

So, the final results set as initial values for the numerical modelization on COMSOL Multyphysics® are:

	$CO_2$	$CO$	$CH_4$	$H_2$
<i>%vol., humid syngas</i>	44.11	36.6	$8.16 \cdot 10^{-3}$	0.97

Table 2. Volumetric percentage of species contained in the humid syngas

Starting from these input values, now, it is possible to evaluate the Low Heating Value (LHV) at 25 °C of the syngas multiplying them with the respective LHV of the substance that acts as fuel in the mixture ( $CH_4$ ,  $H_2$  and  $CO$ ).

The resulting syngas LHV value is 106.05 kJ/mol at 25°C.

## 3 Studied tubular geometry and material properties

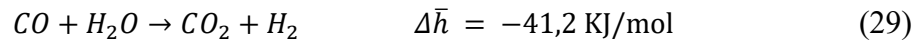
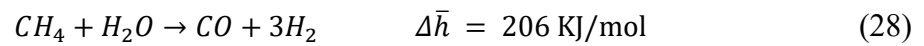
### 3.1 SOFC tubular cell in our project: geometrical description

In the context of the DB-SOFC project, the cell under investigation is an electrolyte-supported tubular cell. It has a length of 16 cm and it is composed by an anode of thickness of 30  $\mu\text{m}$  on the external surface of the tube that develops electrons from the reaction of CO and H<sub>2</sub> produced by the gasification of the biomass.

The two reactions involved are:



Moreover, at the anode occurs also the endothermic reaction of steam methane reforming (SMR) (Eq. 28) and the exothermic water gas shift (WGS) (Eq. 29) reported below with their corresponding values of the variation of enthalpy at 298 K.



The material of which the anode is composed is the CERMET<sup>®</sup>, a particular alloy of yttria-stabilized zirconia (YSZ) and nichel who acts as catalyst for the reactions that occur at the anode.

Instead, on the internal surface of the cell there is the cathode of 30  $\mu\text{m}$  in which the oxygen atoms, contained in the air flow provided by this side, react with the electrons flowing from the anodic side via an electrical connection between the two electrodes in the reaction:



The cathode is formed by Lanthanum Strontium Manganite (LSM), a particular type of perovskite material able to conduct current.

The air needed to the cathodic reaction is injected with a tube of 1 cm of diameter in which the air, from the top of the cell, is carried to the bottom and go back to the top of the cell carrying out the reaction along the cathode.

The two electrodes present a porous structure able to guarantee the flow of the fuel, or air, from the flow channels of the respective side to the electrode-electrolyte interface where the reactions will take place and this structure permits also the exiting of the species produced by the electrochemical reaction.

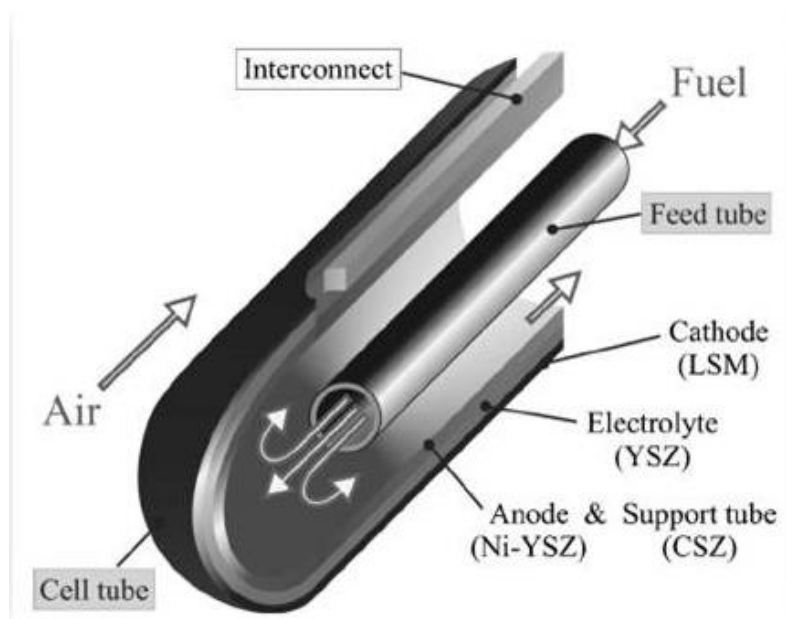


Figure 8. Cathodic air injection design

Between the two electrodes there is the electrolyte that constitutes the tube and in which pass the  $O^{2-}$  ions involved in the reaction, the material which is made of is the yttria-stabilized zirconia (YSZ) and presents a thickness of 1 mm.

The total diameter of the cell results to be of 2 cm.

In the Table 3 and Table 4 are summarized the material properties of each layers of a single cell.

### **Anode – Ni-YSZ**

<i>Density [g/cm<sup>3</sup>]</i>	6.4 [9]
<i>Electrical conductivity [S/m]</i>	$\sigma_{an} = \frac{95 \cdot 10^6}{T} * \exp\left(-\frac{1150}{T}\right)$ [10]
<i>Ionic conductivity [S/m]</i>	- <sup>2</sup>
<i>Specific Area [m<sup>2</sup>/g]</i>	80 [11]
<i>Permeability [m<sup>2</sup>]</i>	10 <sup>-12</sup> [10]
<i>Tortuosity</i>	3 [12]
<i>Porosity</i>	0.3[13]

### **Cathode - LSM**

<i>Density [g/cm<sup>3</sup>]</i>	5 [10]
<i>Electrical conductivity [S/m]</i>	$\sigma_{cat} = \frac{42 \cdot 10^6}{T} * \exp\left(-\frac{1200}{T}\right)$ [10]
<i>Ionic conductivity [S/m]</i>	6.3*10 <sup>-2</sup> [14]
<i>Specific Area [m<sup>2</sup>/g]</i>	80 [11]
<i>Permeability [m<sup>2</sup>]</i>	10 <sup>-12</sup> [10]
<i>Tortuosity</i>	5 [13]
<i>Porosity</i>	0.335[13]

Table 3. Material properties of the electrodes

### **Electrolyte - YSZ**

<i>Electrical conductivity [S/m]</i>	1.75*10 <sup>-2</sup> [15]
<i>Ionic conductivity [S/m]</i>	$3.34 * 10^4 * \exp\left(-\frac{10300}{T}\right)$ [10]
<i>Density [g/cm<sup>3</sup>]</i>	5,16[16]
<i>Poisson's Ratio</i>	0.3 <sup>3</sup>

Table 4. Material properties of the electrolyte

<sup>2</sup> I assume this quantity is the same of the electrolyte because the principal material is the same

### 3.2 Stack description

In conclusion, 25 cells of the type described in the paragraph 3.1 are assembled on a stack in two configurations (Figure 9) for the comparison between them: the first one consists on assembling the cells to form a 5x5 structure on a square stack, in which 5 cells are connected in series and, then, the resulting 5 rows are linked in parallel, the distance between the centers of the cells is 5 cm and the length of the side of the total stack, including the thickness of the walls of it, is 32 cm; the second one is a circular configuration with a total external diameter of 36,28 cm. The cells along the y-axis and the x-axis have a distance between the centers of them of 6 cm and the cells in the middle are in the coordinate: (3 cm, 3 cm), (9 cm, 3 cm), (6 cm, 6 cm) and (3 cm, 9 cm).

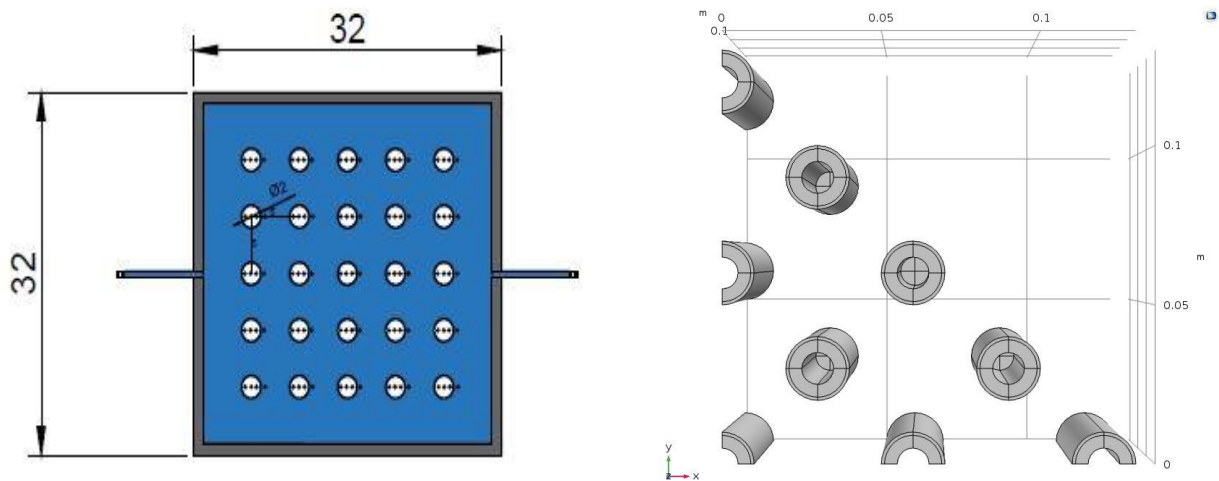


Figure 9. Squared stack geometry (on the left) and circular stack geometry (on the right, a quarter of it)

Connections between the cells are established by connectors external to the stack, so they can be modified and there isn't the need of interconnectors inside the stack that they would affect the flow of the syngas between the cells.

The biomass is injected in the system by the high and it is moved on the interior of the stack by a distribution screw. For its gasification the gasifying agents ( $\text{CO}_2$  and  $\text{H}_2\text{O}$ ) are introduced from the bottom of the stack and the exhaust syngas is collected from the top of the assembly. Part of the exiting syngas  $\text{CO}_2$  and  $\text{H}_2\text{O}$  contents are recovered and recirculated to utilize them from the gasification process.

For what concerns the heat removal, the first idea was to subtract heat from a water heat exchanger on the top of the cells, but in this thesis it is chosen to develop the water heat exchanger and, then, compare it with one projected with air because with the first hypothesis it was thought that would have arisen problems in the upper part of the stack due to high difference of temperature between the water, that will be maintained at high pressure and at relative low temperature (200-300 °C) to have it in the liquid phase, and upper part of the cell.

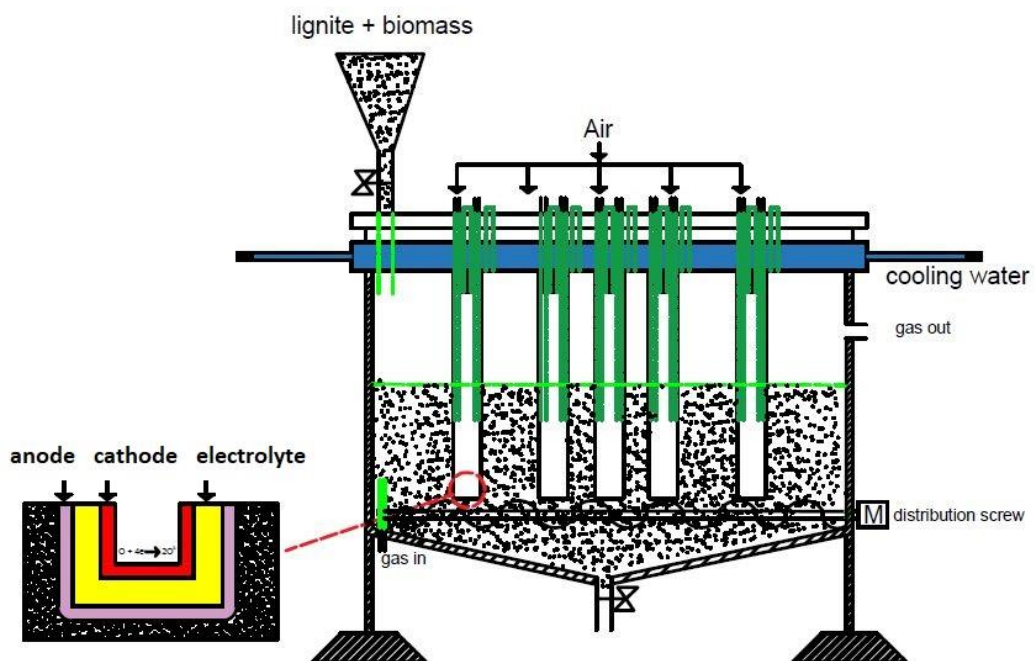


Figure 10. Vertical section of the DB-SOFC stack

## 4 Modelization

The physical model that reproduces the stacks is build on COMSOL Multiphysics. The first pass was to construct the geometry according to the description showed in the third chapter of this work making the hypothesis of dimensionless electrodes to reduce the computational time employed by the software to resolve the system and to limits the problems arisen in the phase of meshing the domains. This hypotesis has been verified with the validation of the work done by my colleague V.Somano in her previous thesis concerning the same project and the results obtained from this validation will be explained in the paragraph 5.1 of this work.

Furthermore, it is necessary to assume generic hypothesis for the development of the model:

- Steady-state conditions
- Initial temperature of a single cell sets to 800 °C
- Nominal voltage sets to 0.7 V
- Feeding with only syngas, as if the gasification process was instantaneous
- Laminar flow of the syngas and the air in the flow channels
- Velocity values of the inlet of air and syngas assumed to be equal to operating conditions of the model of V. Somano[17] to make comparison between the models
- The reactant gas mixtures are approximated as ideal gas
- The cooling water temperature is set to 200 °C, that corresponds to a saturation pressure of 15,55 bar, so it could be maintained at higher pressure than this to avoid the evaporation. Instead, the air for the modelization of an alternative cooling system of the stack it has been hypotized at a temperature of 650 °C
- Three linear distribution of temperature assumed for the inlet of the syngas

Subsequently, it has been applied various physic nodes to the geometry to describe completely the phenomenon that will be presented in the details in the next paragraphs.

## 4.1 Electrochemical model

This model is necessary to evaluate the voltage of every cell to estimate the current density,  $i$  [ $A \cdot m^{-2}$ ], of the stack. For starting this evaluation it has calculated the equilibrium potential of the  $H_2$  and  $CO$  reacting at the anode because it has assumed that these will be the only chemical compounds that will react at the anode side. This is a consequence due to the low amount of  $CH_4$  in the syngas composition, so it has been possible to assume that the SMR reaction totally consumes the methane. Instead, due to the WGS reaction is a chemical reaction slower than the SMR, it can't be assumed that the  $CO$  totally reacts in this reaction to form  $H_2$ .

For the equation of the equilibrium potential on the anodic side it has been used the ones formulated by Ni on his articles [12], [18]:

$$E_{H_2} = 1.253 - 0.00024516 * T + \frac{\bar{R} * T}{2 * F} * \ln \left[ \frac{(p_{H_2}) * (p_{O_2})^{0.5}}{(p_{H_2O})} \right] \quad (31)$$

$$E_{CO} = 1.46713 - 0.0004527 * T + \frac{\bar{R} * T}{2 * F} * \ln \left[ \frac{(p_{CO}) * (p_{O_2})^{0.5}}{(p_{CO_2})} \right] \quad (32)$$

in which the factor “2”, before the Faraday's constant, represents the electrons exchanged in the reaction of oxidation of the  $H_2$  and the  $CO$ ;  $p_i$  are the partial pressures of every  $i$  species involved in the reactions divided by the ambient pressure. The last term of the two equilibrium potential, thanks to the properties of logarithm, are splitted in two parts: one with only the partial pressure of species present at the anode and the other with partial pressure of the oxygen.

So, for the equilibrium potential of the cathodic side it has been adopted the formula reported below[19]:

$$E_{O_2} = \frac{\bar{R} * T}{4 * F} * \ln (p_{O_2}) \quad (33)$$

For the current density, the equation used is the Linearized Butler-Volmer

$$i = i_0 * \left( \frac{(\alpha_{an} + \alpha_{cat}) * F}{\bar{R} * T} \right) * \eta \quad (34)$$

in which  $\alpha_{an}^{H_2} = 1.5$  and  $\alpha_{cat}^{H_2} = 0.5$ ,  $\alpha_{an}^{CO} = 0.62$  and  $\alpha_{cat}^{CO} = 0.38$  and  $\alpha_{an/cat}^{O_2} = 0.5$  [20].

Moreover, the activation current density for the anode and the cathode must be evaluated as reported in the article of Andersson et al.[16] and reported below:

$$i_{0,an} = \frac{\bar{R} * T}{Z_{an} * F} * A_{i,an} * \exp\left(-\frac{E_{act,an}}{\bar{R} * T}\right) \quad (35)$$

$$i_{0,cat} = \frac{\bar{R} * T}{Z_{cat} * F} * A_{i,cat} * \exp\left(-\frac{E_{act,cat}}{\bar{R} * T}\right) \quad (36)$$

In the Eq. (35) and (36)  $A_{i,an/cat}$  are the pre-exponential factor and  $E_{act,an/cat}$  are the activation energy of the two electrodes.

The values adopted for the calculation of these quantities are summarized in the Table 5 [16] and, as suggested by the article of Ni[12], the activation current density of the CO reaction at the anode has been supposed to be 40 % of  $i_{0,an}$ .

$A_{i,an}$ [S/m <sup>2</sup> ]	6.54*10 <sup>11</sup>
$A_{i,cat}$ [S/m <sup>2</sup> ]	2.35*10 <sup>11</sup>
$E_{act,an}$ [J/mol]	1.4*10 <sup>5</sup>
$E_{act,cat}$ [J/mol]	1.37*10 <sup>5</sup>

Table 5. Values adopted for the evaluation of the equilibrium current densities

Another important step for the modelization process is the evaluation of the diffusion coefficients of the species involved in the process both at the anode and at the cathode. These coefficients are responsible of the motion in the flow channels and in the porous electrodes, so it is created a gradient of concentration that reduces the potential of every cell owing to the rising of the diffusion overpotential.

For this modelization it is adopted the Fick's model to make as simple as possible the modelization and with a low computational cost.

Another possibility is to implement the model with the Dusty Gas model, but, as said by Gholaminezhad et al.[21], it doesn't suit well the effect of the limiting current density if the fuel utilization is low. Furthermore, in COMSOL the Dusty Gas model is not present.

The alternative choice could be the Maxwell-Stefan model, but on it there isn't the possibility to consider the Knudsen diffusion for the reconstruction of the 2D model with volumetric electrodes.

The formulas adopted for implementing on software the quantities for the diffusion model have been obtained from the research of Ni [18] and are the following

$$D_i^{eff} = \frac{\varepsilon}{\tau} * \left( \frac{1 - x_i}{\sum_{j \neq i} \frac{x_j}{D_{ij}}} + D_i^K \right) \quad (37)$$

in which  $x$  is the molar fraction of the species considered and  $\varepsilon$  and  $\tau$  are, respectively, the porosity and the tortuosity of the material.  $D_i^K$ , that is the Knudsen diffusion coefficient that has to be considered, according to the studies of Andersson et al. [16], if the pore size has the same order of magnitude of the mean free path, is used only in the construction of the 2D model with volumetric electrodes and the formula to evaluate it is:

$$D_i^K = \frac{d_{pore}}{3} * \sqrt{\frac{8 * \bar{R} * T}{\pi * M_i}} \quad (38)$$

with the value of the pores diameter ( $d_{pore}$ ) is assumed to be  $0.68 \mu\text{m}$  [16] and  $M_i$  is the molar mass of the species taken into account.

The term  $D_{ij}$ , in  $\text{cm}^2/\text{s}$ , is the binary diffusion coefficient estimated as[22]:

$$D_{ij} = \frac{0.0026 * T^{1.5}}{p * \sqrt{\frac{2 * M_i * M_j}{M_j + M_i}} * \left( \frac{\sigma_i + \sigma_j}{2} \right)^2 * \Omega_D} \quad (39)$$

$p$  is the pressure, in bar, of the total mixture containing the chemical species analyzed,  $M_{i/j}$  are the molar mass in kg/mol and  $\Omega_D$  is a dimensionless diffusion collision estimated as:

$$\Omega_D = \frac{1.06036}{B^{0.1561}} + \frac{0.193}{\exp(0.47635 * B)} + \frac{1.03587}{\exp(1.52996 * B)} + \frac{1.76474}{\exp(3.89411 * B)} \quad (40)$$

where

$$B = \frac{k_b * T}{\sqrt{\varepsilon_i * \varepsilon_j}} \quad (41)$$

$k_b$  is the Boltzmann's constant ( $1.38066 * 10^{-23}$  J/K) and the values of  $\sigma_{i/j}$  and  $\varepsilon_{i/j}$ , reported in Table 6, have been procured on literature.

	<i>CO</i>	<i>CO<sub>2</sub></i>	<i>H<sub>2</sub></i>	<i>O<sub>2</sub></i>	<i>CH<sub>4</sub></i>	<i>N<sub>2</sub></i>	<i>H<sub>2</sub>O</i>
$\sigma_i [\text{\AA}]$	3.69	3.941	2.827	3.467	3.758	3.798	2.641
$\varepsilon_i/k_b [K]$	91.7	195.2	59.7	106.7	148.6	71.4	809.1

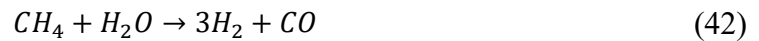
Table 6. Values of  $\varepsilon_i/k_b$  and  $\sigma_i$  found on literature

From these value is now possible to evaluate the diffusion coefficients of every species and the formula are implement in the software through the COMSOL built-in node *Transport Properties* of the physic *Transport of Concentrated Species*.

## 4.2 Steam methane reforming and water gas shift reactions

Another fundamental modelization to take into account is the reforming of the methane contained in the syngas and the shift reaction that occur at the anode. The reactions of SMR (41) and WGS (42) are wrote below.

The kinetic of these two reactions is shifted towards the products at a temperature of almost 800°C for the SMR and at a temperature of almost 300 °C for the WGS.



I assume that the SMR totally occurs due to the fact in syngas composition the CH<sub>4</sub> percentage is very small and the reaction is favoured by the high temperature at which the SOFC works, but I can't affirm the same for the WGS because it is present more than one third of CO in the syngas derived by OK800 biomass gasified at 800°C and the reaction of WGS isn't favoured by the high temperature. Normally, with the external gasification, there is a WGS reactor that works at temperatures between 200 °C and 300 °C to reduce, as much as possible, the CO amount in the syngas and to increase the quantity of H<sub>2</sub>.

To take into consideration these phenomenon it is necessary to implement on COMSOL Multiphysics® the *Reaction Source* node in the *Transport of Concentrated Species* physics applied to the anode side with the values of volumetric rate of reactions for every species which contributes to the electrochemical reactions.

For this purpose, I have calculated, as follows, firstly the equilibrium constant of both reactions with the equations proposed by Haberman et. al[7] derived by experimental tests.

$$K_{pr} = 1.0267 * 10^{10} * \exp(-0.2513 * Z^4 + 0.3665 * Z^3 + 0.5810 * Z^2 - 27.134 * Z + 3.2770) [Pa] \quad (44)$$

$$K_{ps} = \exp(-0.2935 * Z^3 + 0.6351 * Z^2 + 4.1788 * Z + 0.3169) \quad (45)$$

in which

$$Z = \frac{1000}{T} - 1 \quad (46)$$

and, subsequently, the forward catalysed reaction rate constants

$$k_{r,forward} = 2395 * \exp\left(-\frac{231266}{\bar{R} * T}\right) \quad (47)$$

$$k_{s,forward} = 0.0171 * \exp\left(-\frac{103191}{\bar{R} * T}\right) \quad (48)$$

Finally, it is possible to obtain also the backward ones thanks to the relation of the two catalysed reaction rate constants with the corresponsive equilibrium constant.

$$K_{pr} = \frac{k_{r,forward}}{k_{r,backward}} \quad (49)$$

$$K_{ps} = \frac{k_{s,forward}}{k_{s,backward}} \quad (50)$$

Now, knowing also the backward catalysed reaction rate constants and the partial pressure of the species involved in every reaction, I'm able to estimate both the volumetric rate of reaction that are expressed in  $[\text{mol m}^{-3} \text{s}^{-1}]$  [23]

$$R_r = k_{r,forward} * p_{CH_4} * p_{H_2O} - k_{r,backward} * p_{CO} * p_{H_2}^3 \quad (51)$$

$$R_s = k_{s,forward} * p_{CO} * p_{H_2O} - k_{s,backward} * p_{CO_2} * p_{H_2} \quad (52)$$

In conclusion, the molar rates of formation can be formulated as follows and multiplied by the molar mass of the species taken into account so, they are expressed in  $[\text{kg} * \text{m}^{-3} * \text{s}^{-1}]$ .

$$\left\{ \begin{array}{l} R_{CH_4} = -R_r * M_{CH_4} \\ R_{CO} = (R_r - R_s) * M_{CO} \\ R_{CO_2} = R_s * M_{CO_2} \\ R_{H_2O} = (-R_r - R_s) * M_{H_2O} \\ R_{H_2} = (3 * R_r + R_s) * M_{H_2} \end{array} \right. \quad (53)$$

### 4.3 Heat management

For what concerns the modelization of the heat transfer it is implemented on COMSOL the physic node *Heat transfer in Solids* that describes the heat transfer with the formula

$$\rho * c_p * \mathbf{u} * \nabla T + \nabla \mathbf{q} = \mathbf{Q} \quad (54)$$

in which  $\mathbf{u}$  is the velocity vector in m/s,  $\rho$  is the density of the gas in kg/m<sup>3</sup>,  $c_p$  is the specific heat capacity of the gas [J/kg\*K] and  $\mathbf{Q}$  is the thermal source/sink in W/m<sup>3</sup>.

Furthermore,  $\mathbf{q}$  is the conductive heat flux and it can be evaluated as:

$$\mathbf{q} = -k * \nabla T \quad (55)$$

Then, the boundary conditions has to be implemented and, initially, are inserted two Dirichlet boundary conditions that represents the inlets of air and syngas in the *Temperature* node.

In the model, the convection contribute is considered introducing the velocity field term of the two fluids that flow in the cathodic and the anodic flow channels.

To take into account also the heat generated, or absorbed, by the WGS and SMR it is inserted an heat source boundary condition in which are summed the WGS heat generation contribution and the SMR endothermicity starting from

$$\begin{cases} H_{SMR} = -(206205.5 + 19.51 * T) & \left[ \frac{J}{mol} \right] \\ H_{WGS} = 45063 - 10.28 * T & \left[ \frac{J}{mol} \right] \end{cases} \quad (56)$$

and multiplying each contribution with the respective rate of reaction  $R_r$  and  $R_s$  calculated in the previous paragraph. [12], [16]

In addition, the heat is generated due to three contribution: heat generated by Joule heating in the cell, heat derived by the irreversibilities of the reaction that occurred at the anode electrode and heat generated by the activation of the electrochemical reaction.

The first of this is inserted in the model using a domain *Heat Source* in the electrolyte that calculates the total power dissipation density inside it. The activation of the reaction is taken into consideration putting a boundary condition for the anode and the cathode electrode in the *Multiphysics* node called *Boundary Electrochemical Heat Source*.

The heat generated by the irreversibilities are estimated evaluating the entropy changes in the electrochemical reaction of hydrogen and carbon monoxide.

For the evaluation of the entropy differences it has been obtained from the Nist-Janaf Thermochemical Tables the values of entropies of the species involved in the two electrochemical reactions at the anode. These values are reported in the Table 7 for the operative temperature of 800 °C. Then, the values of entropies of the database are plotted on Excel to obtain a curve, that is function of the temperature, of every reactants, or products, of the reactions. The fitting is always done with a fitting curve of the type “exponential”. In the end, the heat source is implemented in the software with the node *Boundary Heat Source*.

<b>S<sub>H2</sub></b> <b>(kJ/molK)</b>	<b>S<sub>H2O</sub></b> <b>(kJ/molK)</b>	<b>S<sub>CO</sub></b> <b>(kJ/molK)</b>	<b>S<sub>CO2</sub></b> <b>(kJ/molK)</b>	<b>S<sub>O2</sub></b> <b>(kJ/molK)</b>
166.83	236.06	236.34	274.15	245.83

Table 7. Entropies at temperature of 1073 K

At the end, to fill completely the model the specific heat capacity and the conductivity of each material must be inserted in the software. These values are reported in the Table 8.

### **Anode – Ni-YSZ**

<i>Thermal conductivity, <math>k_{AN}</math> [W/mK]</i>	11
<i>Specific Heat, <math>c_{p,AN}</math> [J/kgK]</i>	450
<b>Electrolyte - YSZ</b>	
<i>Thermal conductivity, <math>k_{ELY}</math> [W/mK]</i>	2.7
<i>Specific Heat, <math>c_{p,ELY}</math> [J/kgK]</i>	470
<b>Cathode - LSM</b>	
<i>Thermal conductivity, <math>k_{CAT}</math> [W/mK]</i>	6
<i>Specific Heat, <math>c_{p,CAT}</math> [J/kgK]</i>	430

Table 8. Thermal parameters of every layer composing the cell [16]

The heat generated is managed with a cooling system on top of the stack and in this work it is designed in two ways: the first one with water at 200 °C and at a pressure of 18 bar (assumed to be higher than the saturation pressure), to avoid the evaporation of the fluid, and the second one with air at 650 °C.

The modelization of the cooling system is conducted inserting in the model builder of COMSOL an another *Boundary Heat Source* node choosing the option of a convective heat flux in which are inserted the values of the fluid temperature and the heat transfer coefficient. For the evaluation of this last parameter it has been used the correlation proposed by Dittus-Boelter supposing the fluid flows on a non-circular tube with an equivalent diameter of 0.03 m, that is the same value of the total diameter of the anode channel.

$$Nu = 0.023 * Re^{0.8} * Pr^{0.3} = \frac{h * D_{eq}}{k} \quad (57)$$

$$Re = \frac{\rho * v * D_{eq}}{\mu} \quad (58)$$

$$Pr = \frac{c_p * \mu}{k} \quad (59)$$

Values of fluid properties are obtained at temperature hypotized for the fluid: 200 °C for water and 650 °C for air.

Values of velocity are assumed to be 1 m/s for water and 10 m/s for air and the values of the equivalent diameter is assumed to be equal to all the diameter of the anode flow channel modelized (3 cm).

From the equations above is, now, possible to determine the heat transfer coefficient for the two cooling systems: the results are  $8370 \text{ W}\cdot\text{m}^{-2}\cdot\text{K}^{-1}$  for the water cooling system and  $161 \text{ W}\cdot\text{m}^{-2}\cdot\text{K}^{-1}$  for the air cooling system.

## 5 Results

### 5.1 2D model validation

Before the effective modelization of the stacks, it has been necessary, as already said, to verify the consistency of the approximation of the electrodes. This has been possible with the reconstruction of the cross-section of the cell in 2D modelizing the electrodes as dimensionless domains (edges) in which the reactions take place and the only 2D domains are the cathodic and anodic flow channels and the electrolyte. Moreover, the modelization is done without taking into account the carbon deposition, that could influence the performance of the cell and all the quantities involved in the process are estimated at the operational temperature (800°C) due to the fact the temperature gradients with respect to the reference temperature are expected to be less than 20°C in all the three domains. [17]

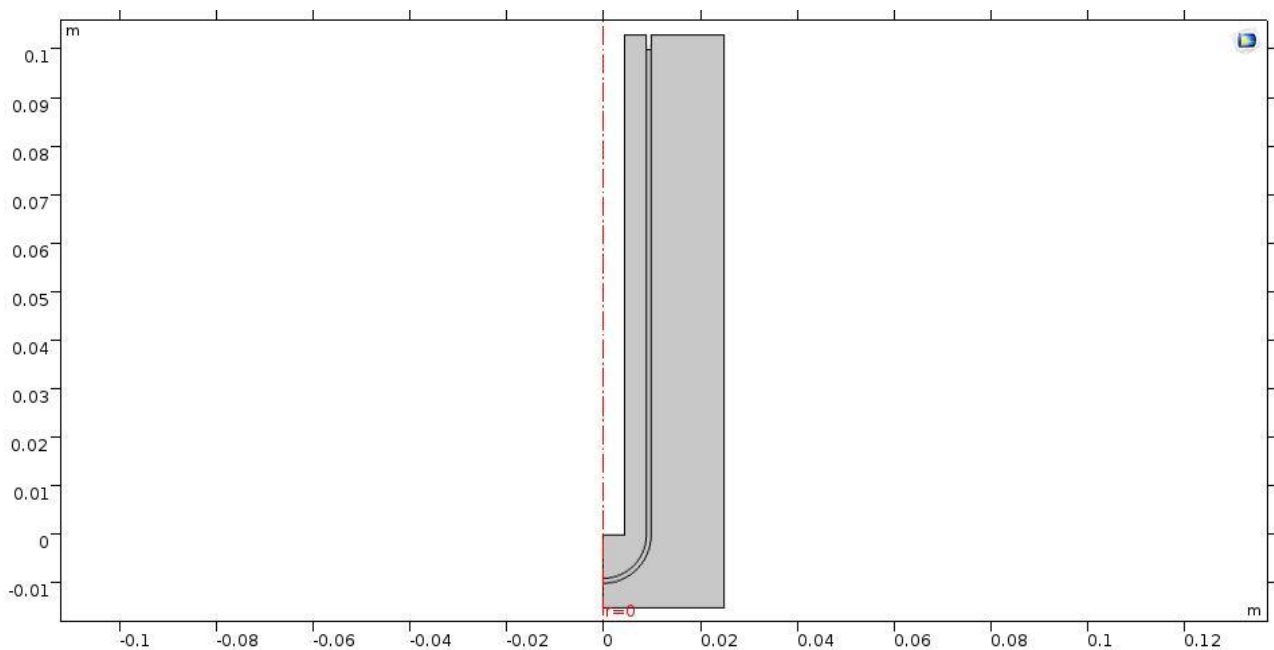


Figure 11. 2D cross-sectional view of the cell with length of 11 cm

The model has been computed with two different meshes to verify that the error with respect to the model without the approximation is due to the different construction of the electrodes or due to computational errors caused by different quality of the chosen mesh.

So, after the computation of this new model it has been possible to plot the polarization curves obtained with a coarser mesh (grey line) and a normal mesh (blue line). As showed in the Figure 12, the two curves are identical and, at the operational voltage, the cell provides a current density of almost  $1245 \text{ A}\cdot\text{m}^{-2}$  and the point is located in the linear region of the polarization curve.

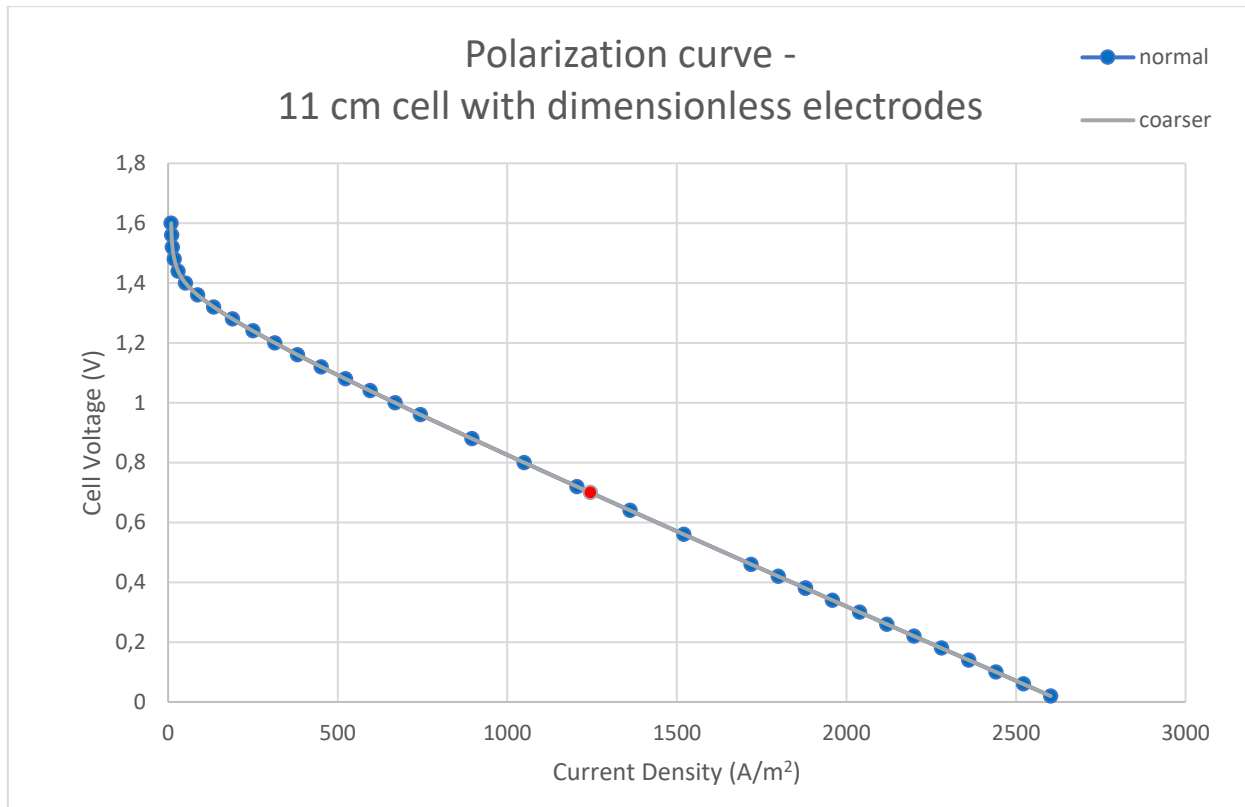


Figure 12. Polarization curves of the 2D model with the approximation of the electrodes

In conclusion, it has been plotted the power density curve for the 2D cell in Figure 13 and the resulting power density output of the cell amounts to almost  $871 \text{ W}\cdot\text{m}^{-2}$ , that corresponds to a power of 6.0 W. The point of functioning results to be near the Maximum Power Point.

The resulting efficiency for this configuration, calculated applying the Eq. 20, will be of 5 % but this value isn't influenced by the Fuel Utilization because to obtain this value it has been used at the denominator of the efficiency formula the amount of syngas that enter inside the bottom of the anodic channel (see Figure 11). Thus, the result of efficiency obtained has been divided by the calculated FU, that amounts to 10.6 %, and therefore the electrical conversion efficiency, considering only the effective syngas that interacts with the anodic electrode, will be of 47.9 %.

From the cathodic side, instead, the calculated AU results to be 26.75 %.

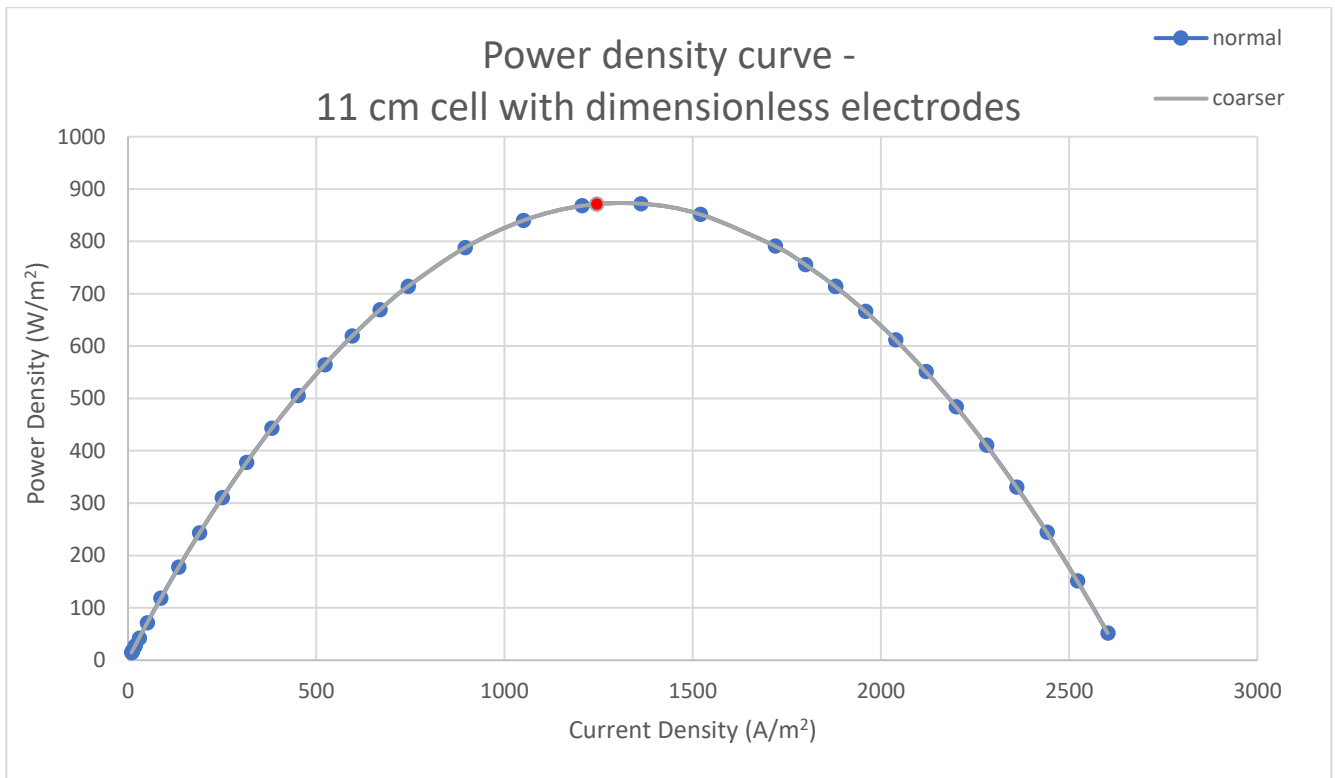


Figure 13. Power density vs. current density curve of the 2D cell

Comparing the result obtained from the model with the approximation introduced and the original modelization conducted by V.Somano, comes out a significant difference between the two power output. The difference amounts to almost 3.5 W and it could come out because she chooses a ionic conductivity of 180 S/m and low values of electronic conductivity for the electrodes[17]. The difference couldn't be caused by the lack of dependency on temperature because re-computing the model with all properties evaluated at 820 °C comes out a power of 6.15 W.

To be sure that the difference derives only by the different values adopted for the ionic conductivity, it has been necessary to reconstruct the 2D model with the volumetric electrodes. In this model the adopted data are the ones reported in Tables 3 and 4. The thickness of the anodic/cathodic GDL amount to  $1.95 \cdot 10^{-5}$  m and the anodic/cathodic catalyst layer have got a thickness of  $1.05 \cdot 10^{-5}$  m.

From this new model comes out a current density of  $1256.4 \text{ A} \cdot \text{m}^{-2}$  that corresponds to a generated power of 6.07 W. This results differs from 2D model with dimensionless electrodes of 1.3 %, so the approximation of the electrodes is acceptable and it would be used for the following simulation.

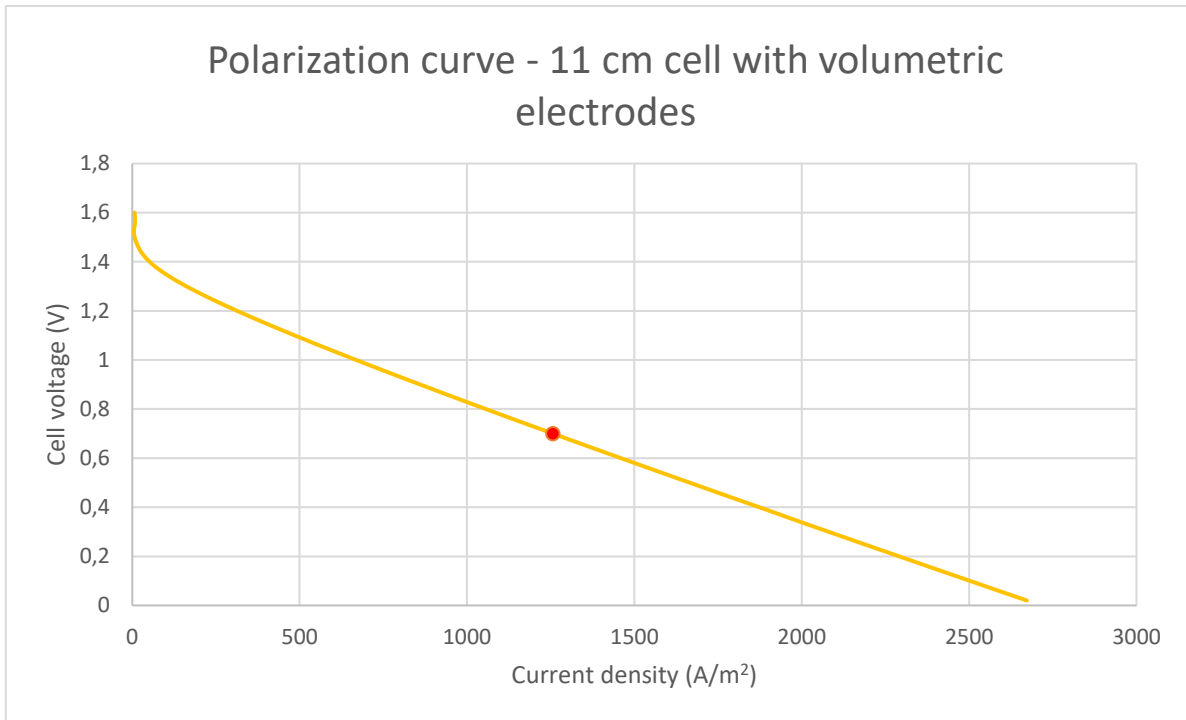


Figure 14. Polarization curve of the 2D model built with volumetric electrodes

From the plots, it can be recognized only the first region of the curve that is the one in which the activation overpotential occurs. The third region is not present because, as for the PEMFC<sup>3</sup>, the curve is influenced by the low value of the transfer coefficient, in particular from the one of the CO that mainly influence the behaviour of the polarization curve because there is a high amount of it in the syngas.

<sup>3</sup> <https://www.sciencedirect.com/topics/engineering/polarization-curve>

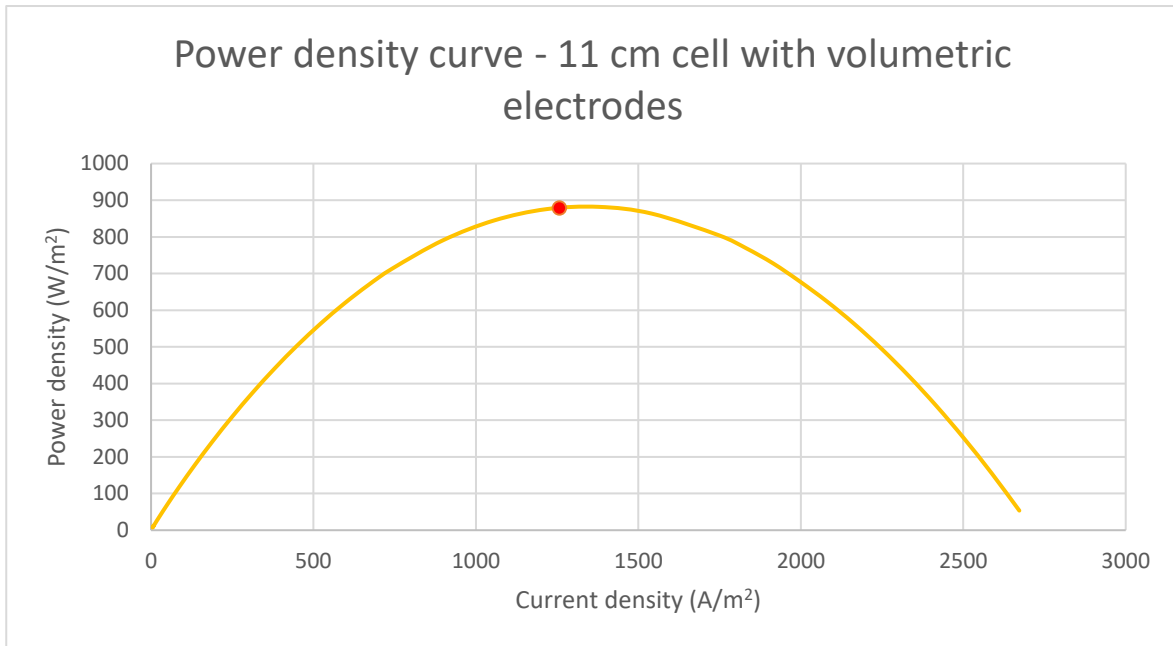


Figure 15. Power density curve of the 2D model built with volumetric electrodes

Consequently, it has been decided to increase the length of every cell to harness an high reacting surface and, so, to reach the project goal of 8 W already on isothermal condition.

## 5.2 Reconstruction of the 2D cell with a length of 16 cm

As said, during the development of the project it has been decided to change the length of every cell and to bring it to a value of 16 cm. So, another validation is required and, as expected, with this length it has been obtained a current density, and the relative power output, acceptable for the purpose of the project as showed in the polarization curve, relative to this validation, reported in Figure 16. As it can be noticed, in the polarization curve there is, as in the previous validation, only the zone of activation overpotential and the linear region.

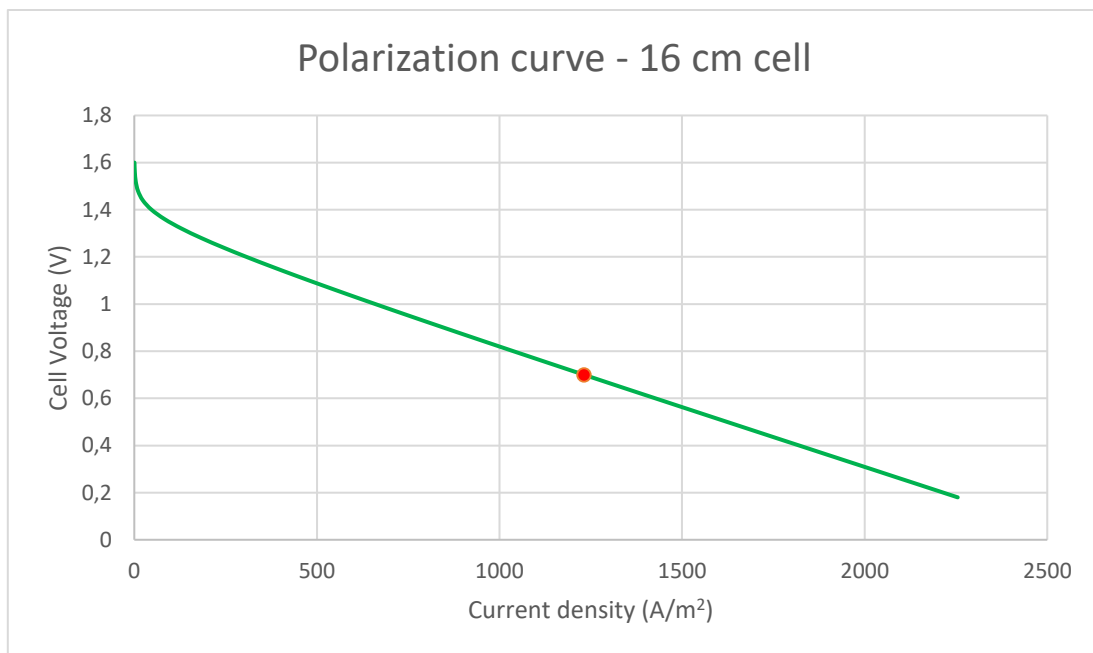


Figure 16. Polarization curve of a single 16 cm cell

From the graph it can be extracted the current density developed from the cell at the nominal condition (0.7 V in this work). The value obtained is 1231 A\*m<sup>-2</sup> that corresponds to a power of 8.66 W. This results is obtained with a relative tolerance sets to 10<sup>-3</sup> and using a coarser mesh to reduce the computational cost, because, as seen before, there aren't significant variation between results with different types of mesh. The value is higher than the goal of the project so it can be accepted since in the model the electrodes has been approximated.

Also in this case the operational point is near the Maximum Power Point and the corresponding power density can be extracted by the power density vs. current density curve plotted in Figure 17.

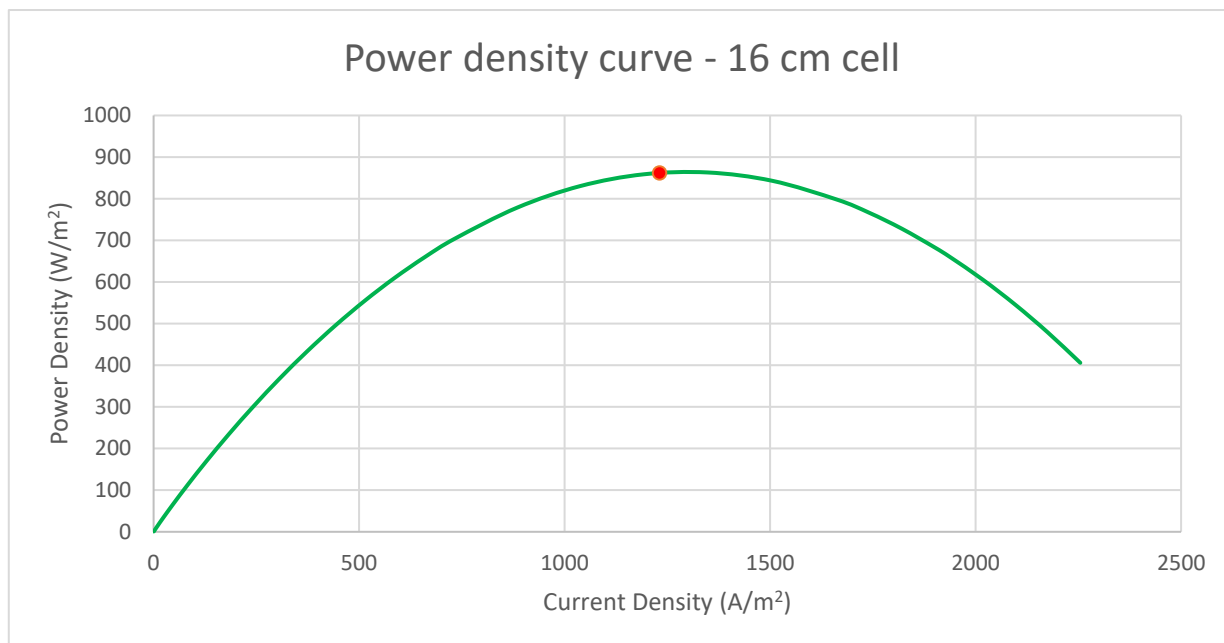


Figure 17. Power density curve of a single 16 cm cell

Also in this case it has been calculated the efficiency and the fuel utilization in this configuration and they are, respectively, 7.33 % and 15.3%. So, the resulting electrical conversion efficiency is 47.9 %. This last value represents, as told in the previous paragraph, the efficiency of conversion of the syngas, that effectively reaches the reaction zone, into electricity through the electrochemical reactions.

For what concern the AU calculated on the cathodic side results to be 38.6 %.

Therefore, considering the cell always at 800° C, it could be extracted a power higher than the goal of the project only in the case the cell is 16 cm long.

## 5.3 Development of the 3D model

Subsequently, it has been developed a 3D model of a single cell to notice if there would be meaningful differences in the passage from 2D to 3D modelization. The mesh adopted, to not load on the computational cost, is a coarser one.

In this part of the thesis has been constructed two different configuration of the cell of a length of 16 cm with the anode channel with a radius of 1.5 cm, as suggested in the thesis of V. Somano[17] in the part of optimization of the cell. The two models differ from the methods of heat removal and are modelized as described in the paragraph 4.2; the results for both of them are reported in the next paragraph.

### 5.3.1 Performance of the 3D cell with water heat removal system

With this type of heat removal system it was found the cell can provide a current of 16.521 A that corresponds to a power density of  $1150.7 \text{ W}\cdot\text{m}^{-2}$ , so the resulting power output will be of 11.57 W. This provided power is higher than the 2D simulation because in this case it has been considered the dependency of the system on temperature; instead, for the 2D simulation all the quantities are calculated at the operative temperature of  $800^\circ\text{C}$ , since the expected gradient was low (almost  $20^\circ\text{C}$ ), as suggested by V.Somano[17]. Re-computing the 3D cell model without taking into consideration the temperature dependency, so the quantities are again calculated at  $800^\circ\text{C}$ , and the result is 9.5 W of electrical power. From these evaluation, comes out that there is a difference of 0.84 W (+9.7 %) from the 2D to 3D modelization.

In the complete 3D model, also the AU increases to a value of 51.57 %, because the ionic conductivity undergoes an increment proportional to the temperature, so the air and fuel are better harnessed. The fuel utilization, in this case, reaches the values of 56.80 %.

Therefore, also the overall efficiency increases to the value of 27.18 % but the electrical conversion efficiency remains unchanged (47.85 %).

The velocity profile of the two fluid, syngas and air, are reported in the following figure (Figure 18) and, as expected, the syngas velocity increases along the flow channel because of the section reduction of it, instead the air velocity undergoes a reduction along the cathodic flow channel for the deviation of its pathway due to the inlet and the outlet of air are both in the upper part of the cell.

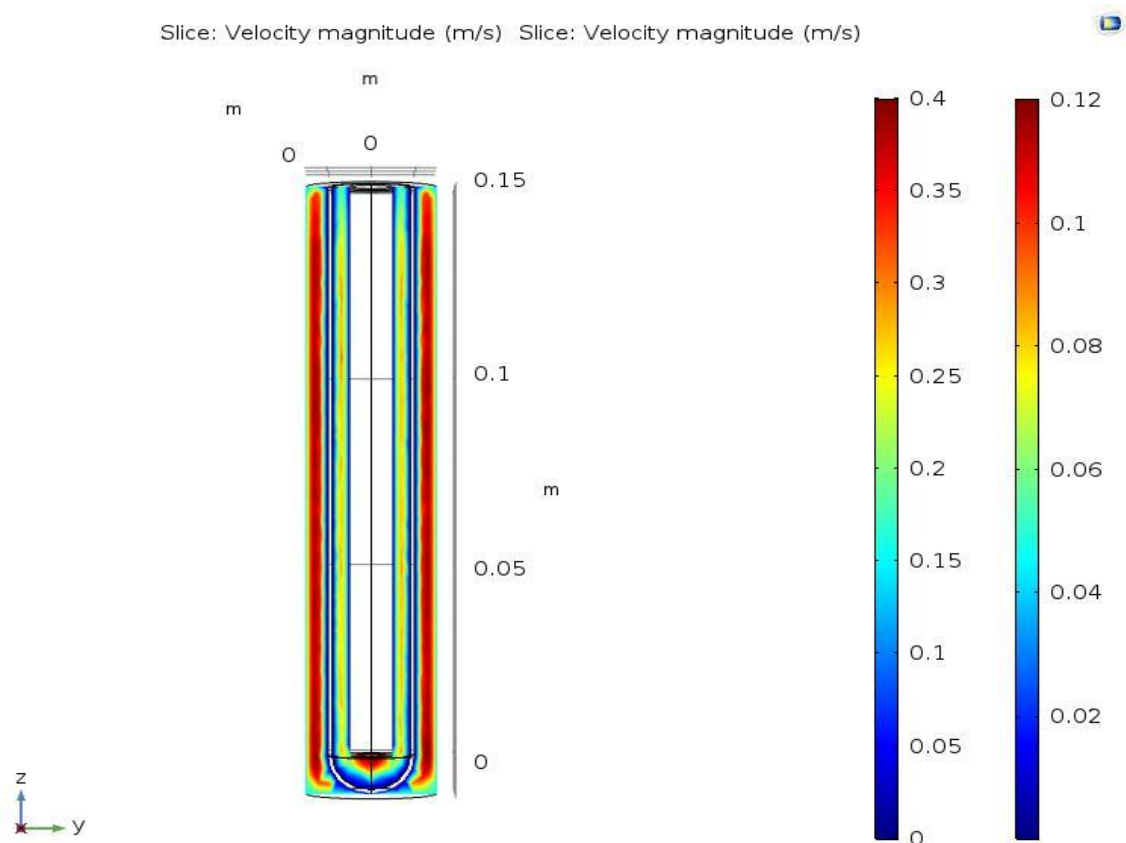


Figure 18. Velocity profiles of syngas and air in the 3D cell cooled by water (the right legend is the one for the syngas)

The temperature distribution inside the cell is illustrated in the Figure 19 and it can be recognized the contact zone between the upper part of the cell and the cooling system: in this zone an high gradient is present, because water must be maintained in liquid state, and it could cause a deactivation of the electrolyte and the resulting power output could undergoes a reduction. Indeed, it may also be that there is a cell rupture and part of the syngas could reach the cathode side causing the cross-over effect.

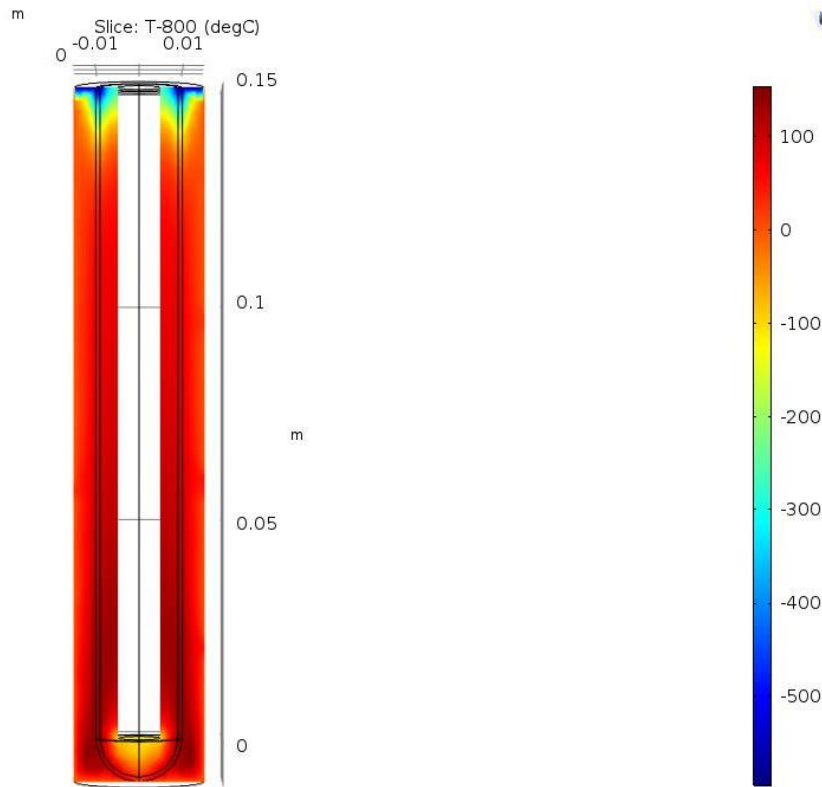


Figure 19. Temperature gradients inside the cell and the flow channels with respect to 800 °C, adopting the water heat removal system

The resulting average temperature in the cell resulted to be 860.7 °C, instead in the internal part of the structure, that is where the air flows, the transfer of heat is slow so in this zone can be recorded an average temperature of 862.95 °C. The average temperature detected in the syngas flow channel is 837.23 °C; These values are heavily influenced by the low temperatures near the heat exchange interface.

The situation is reversed if the maximum temperature are taken into consideration, because the highest value can be found on the syngas flow and it amounts to 961.63°C, instead the other two values are similar: 941.17 °C in the air channel and 941.35 °C in the cell.

For what concern the minimum value of temperature, in the cell it has a temperature of 213.38 °C and 221.68 °C in the air flow channel. For the minimum syngas value, the recorded temperature amounts to 83.922 °C, but I think there was been a computational error, because it isn't possible to have a value below the temperature of water.

Now, it is interesting to see the evolution of  $H_2$  and  $H_2O$  of the molar fraction along the cell height because it can be seen that the production of  $H_2$  and the consumption of  $H_2O$  reach their maximum in the lower part of the cell.

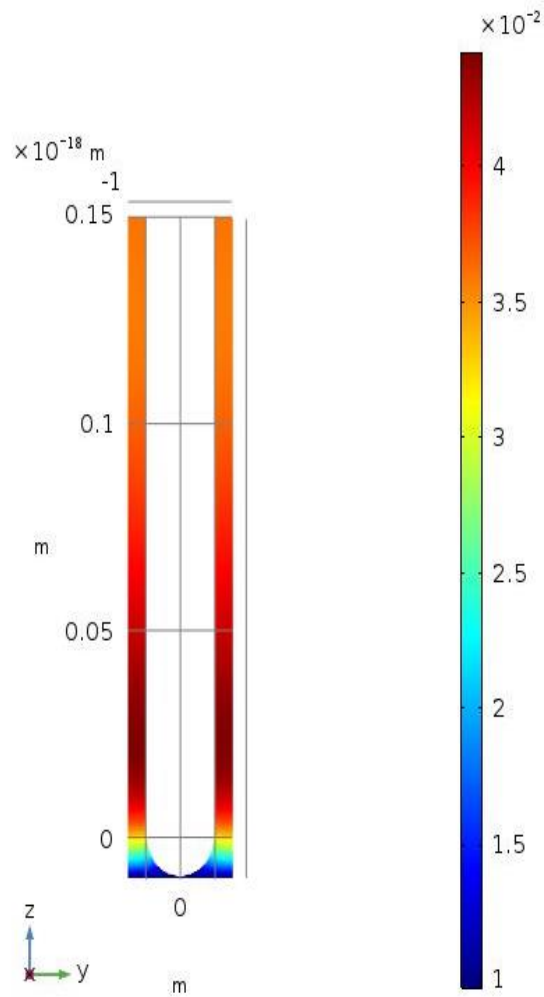


Figure 20. Molar fraction distribution of  $H_2$

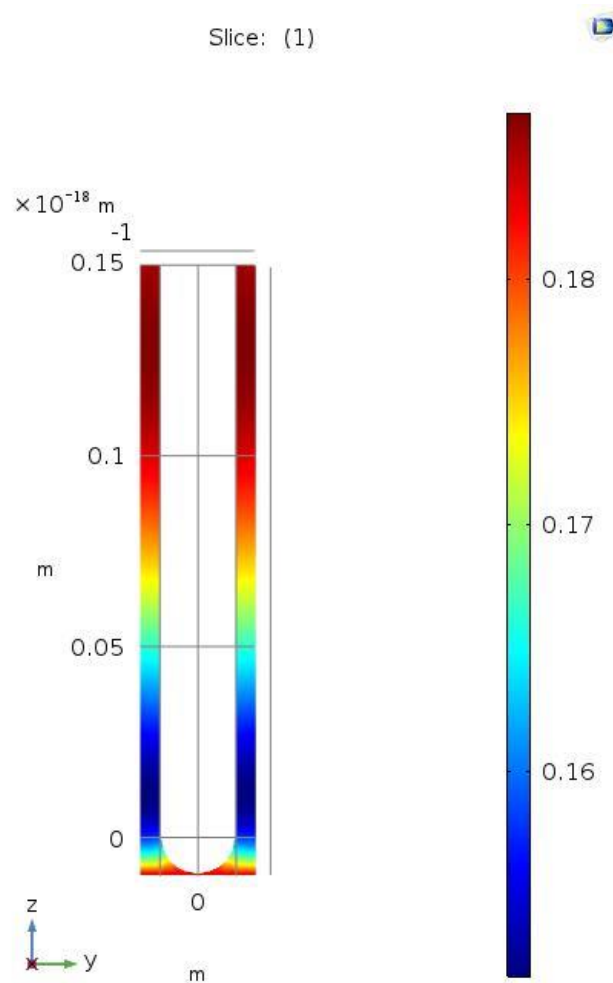


Figure 21. Molar fraction distribution of H<sub>2</sub>O

The other five species involved in the system (CH<sub>4</sub>, CO and CO<sub>2</sub> in anode flow channel and O<sub>2</sub> and N<sub>2</sub> in the cathode flow channel) undergo a continuous decreasing from the respective point of input to the point of exiting.

Instead, CH<sub>4</sub> and CO continuously decrease from the bottom of the cell to the top, because they are only consumed along their pathway; CO<sub>2</sub> molar fraction, since it isn't a reacting species, increases inside the syngas and at the point of extraction it is rich in CO<sub>2</sub> content; part of this CO<sub>2</sub> will be recirculated to make the gasification and the other part could be used in Carbon Capture and Sequestration/Utilization system using the post-combustion, or oxy-fuel, process to make, as much as possible, eco-friendly the whole system. The same behaviour happens on the cathodic side with the consumption of oxygen during its pathway and the resulting increasing of the N<sub>2</sub> molar fraction in the exiting air.

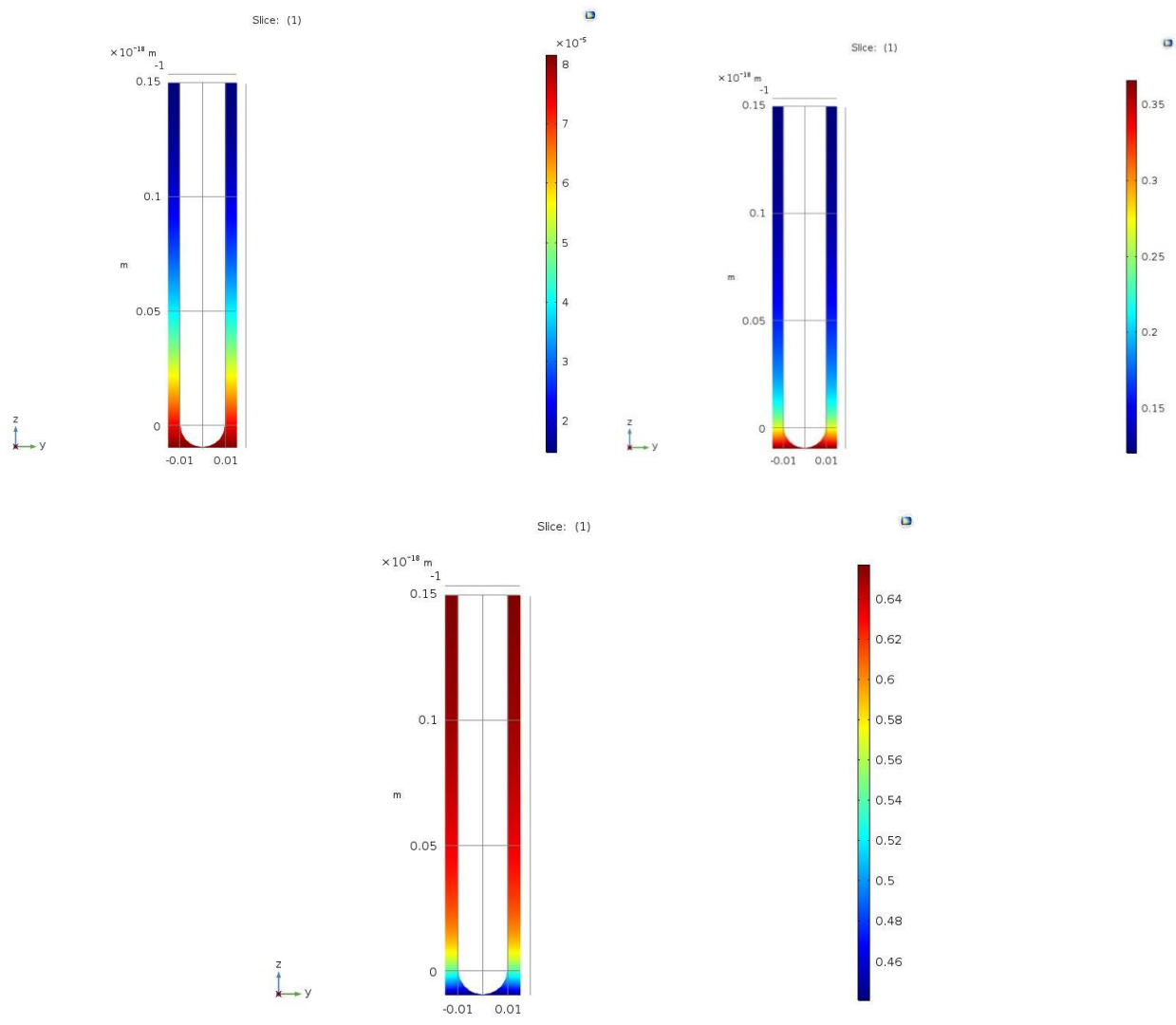


Figure 22. Distribution of chemical species in the anode channel: CH<sub>4</sub> (top left), CO (top right) and CO<sub>2</sub> (bottom)

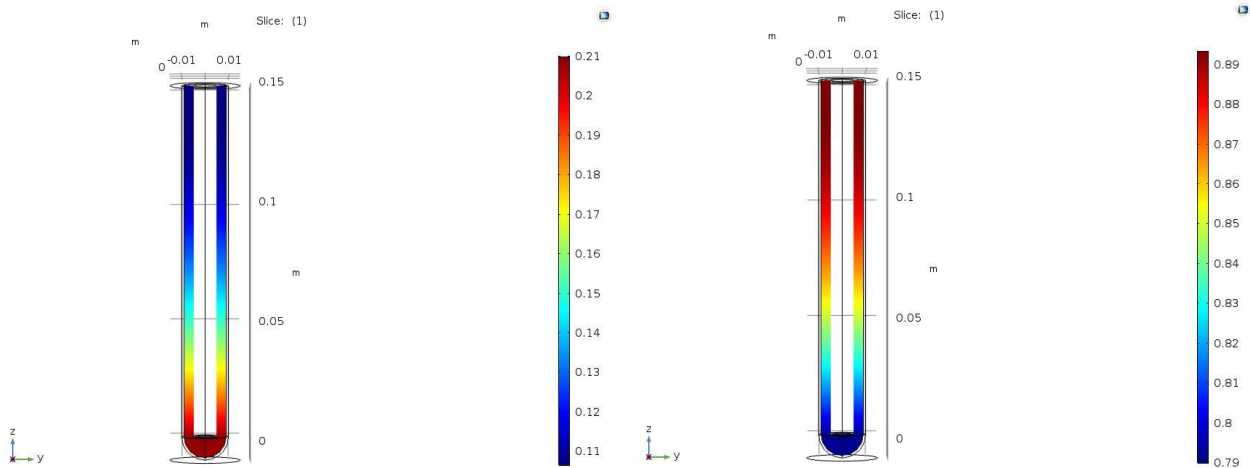


Figure 23. Cathode chemical species distribution: O<sub>2</sub> on the left and N<sub>2</sub> on the right

### 5.3.2 Performance of the 3D cell with air heat removal system

As a consequence of the high gradients of temperature reported in the previous system of heat removing, it has been decided to modelize the cooling system with air at 650 °C to reduce the temperature gradients between the cooling fluid and the interior part of the stack, that could cause a fast degradation of the cell.

From the simulation comes out that the cell is able to provide a power of 12.63 W that corresponds to an increase of 8.4 % with respect to the water cooling system, therefore there isn't a huge difference between the two systems, as supposed before, in terms of power output. The resulting current output, so, amounts to 18.051 A. As a consequence, there is an increase on the efficiency, 29.68 %, on the AU, 56.32%, and on the FU that, now, amounts to 62.0 %.

In this case the temperature distribution that can be observed is reported in the following figure

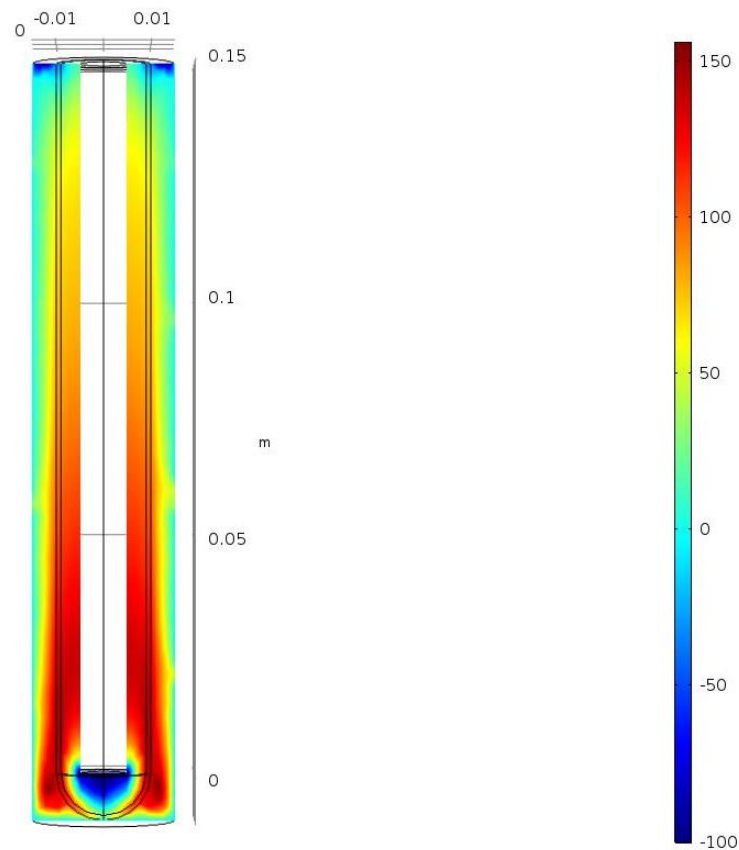


Figure 24. Temperature gradients inside the cell and in the flow channels with respect to 800 °C, adopting the air cooling system

So, as it can be noticed, the temperature is always above the value of 650 °C and it permits to don't have failures and ruptures of the cell.

In this case the average temperature inside the cell results to be 891.89 °C, that is 31 °C higher than the value obtained with the other cooling system; for what concern the syngas average temperature the value is 849.73 °C and the air average temperature is 886.66 °C. The maximum temperature are: 963 °C for the syngas, 945.32 °C for the cell and 945.15 °C for the air.

Instead, in this case, the minimum values of temperature are all above the cooling fluid temperature and amount to: 694.24 °C for the syngas flow, 761.5 °C for the cell and 699.37 °C in the air flow channel.

Then, from the analysis of the distribution of the molar fraction of the anodic species, in particular H<sub>2</sub> and H<sub>2</sub>O, it can be noticed that the cell is able to produce power also in the upper part because there is less H<sub>2</sub> than in the previous case and, as a consequence, an higher amount of H<sub>2</sub>O. These differences on the quantities of these species justify the higher power output.

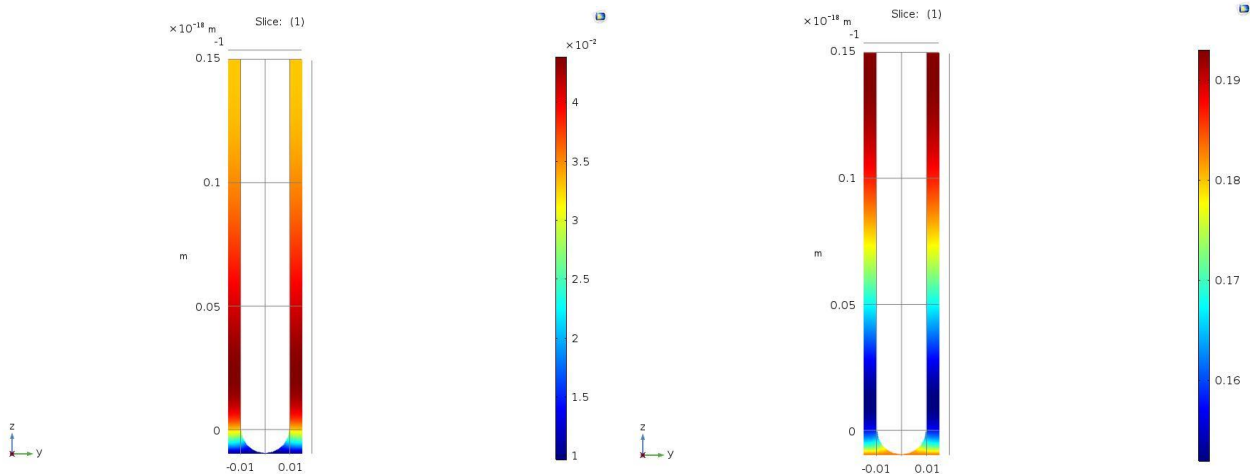


Figure 25. Distribution of the molar fraction of H<sub>2</sub> (left) and H<sub>2</sub>O (right)

The evolution of the other chemical species are similar to the cell cooled by water, because it has got a continuous increase along the z-axis.

### 5.3.3 Comparison between the two cooling systems

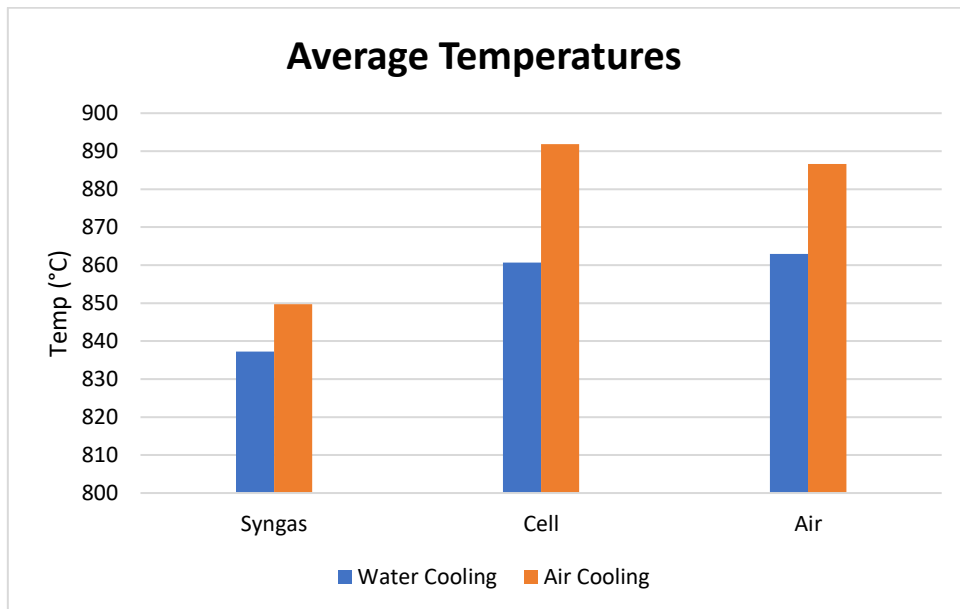


Figure 26. Average temperatures for the two different cooling system

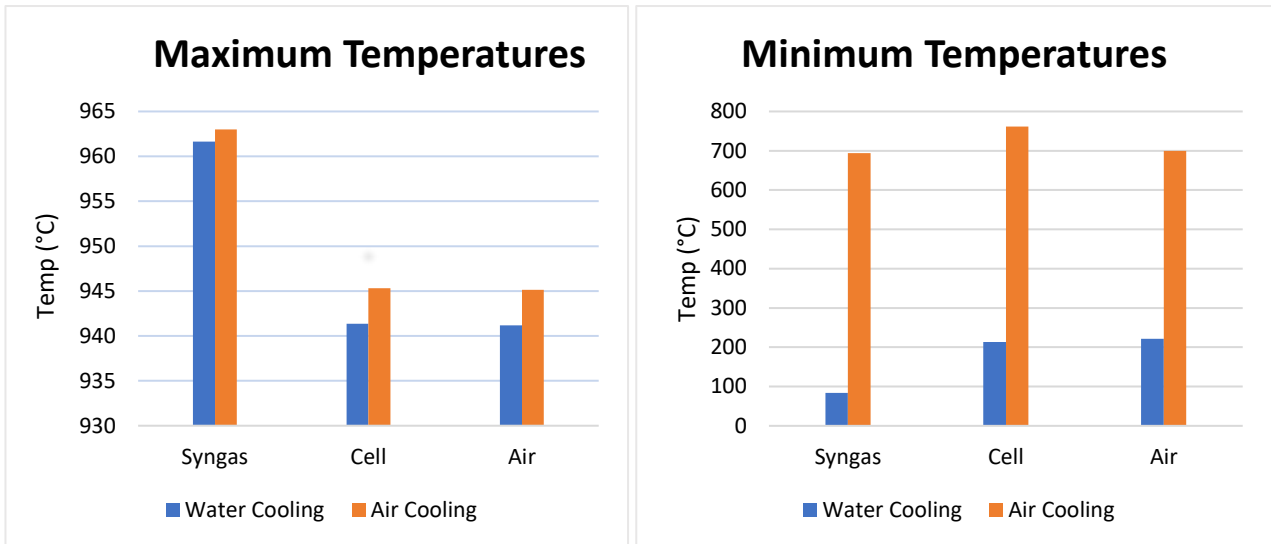


Figure 27. Maximum and minimum temperatures for the two different cooling system

From the graphs above, it can be affirmed that the system reaches similar maximum temperature in all its part and the only difference can be noticed looking at the minimum values that influence the average temperatures and the performance of the cell because, in the case of water cooling system, its ionic conductivity, that follows an exponential function dependent on temperature, sharply decrease reducing the available power output. The maximum values are localized near the emisphere that close the tube, instead, as expected, the minimum value are detected near the contact zone between the cell and the cooling fluid. The maximum temperature are similar in both cases because in the region that they are located, the cooling system fails to subtract heat in an efficient way.

Other important differences can be found on the values of AU, that increases in the cell cooled by air of almost 5 % with respect to the one cooled by water and the FU increases of about 6 %. An another consequence of the power production increment is the increasing of the overall efficiency of 2%.

In conclusion, it can be affirmed that the air cooling system is the best solution to reduce as much as possible the thermal gradients between the top and the bottom of system and at the same time with this configuration it is possible to get almost 1 W more of electrical power.

Subsequently, it has been conducted other simulation introducing different distribution of temperature of the syngas at the inlet of the cell to compare the two cooling system and verify that the air one is always better than the water cooling system.

## 5.4 3D stacks: power and temperature distribution

### 5.4.1 Squared stack

#### 5.4.1.1 OK800: water and air cooling system

Now, three different temperature distribution inside the squared stack has been supposed to analyze the power output that could be extracted from the stack in this three configuration. The distribution has its highest value near the injection of biomass in the stack and the temperature linearly decrease along the stack. Before starting with the evaluation, one needs to evaluate the quantity of the species contained in the syngas at each temperature of the distribution, which will be set as initial values in the simulation.

These values are reported in the tables below

	$X_{0,CH_4}$	$X_{0,H_2}$	$X_{0,CO}$	$X_{0,CO_2}$	$X_{0,H_2O}$
<b>800 °C</b>	$8.168 \cdot 10^{-5}$	$9.72 \cdot 10^{-3}$	$3.66 \cdot 10^{-1}$	$4.41 \cdot 10^{-1}$	$1.832 \cdot 10^{-1}$
<b>787.5 °C</b>	$7.32 \cdot 10^{-5}$	$8.13 \cdot 10^{-3}$	$3.25 \cdot 10^{-1}$	$4.80 \cdot 10^{-1}$	$1.867 \cdot 10^{-1}$
<b>775 °C</b>	$6.48 \cdot 10^{-5}$	$7.29 \cdot 10^{-3}$	$2.83 \cdot 10^{-1}$	$5.19 \cdot 10^{-1}$	$1.90 \cdot 10^{-1}$
<b>762.5 °C</b>	$5.225 \cdot 10^{-5}$	$5.63 \cdot 10^{-3}$	$2.09 \cdot 10^{-1}$	$5.89 \cdot 10^{-1}$	$1.96 \cdot 10^{-1}$
<b>750 °C</b>	$4.0 \cdot 10^{-5}$	$4.80 \cdot 10^{-3}$	$1.68 \cdot 10^{-1}$	$6.28 \cdot 10^{-1}$	$2.0 \cdot 10^{-1}$

Table 9. Temperature distribution of the syngas OK800 and relative species quantities between 800 °C and 750 °C

	$X_{0,CH_4}$	$X_{0,H_2}$	$X_{0,CO}$	$X_{0,CO_2}$	$X_{0,H_2O}$
<b>800 °C</b>	$8.168 \cdot 10^{-5}$	$9.72 \cdot 10^{-3}$	$3.66 \cdot 10^{-1}$	$4.41 \cdot 10^{-1}$	$1.832 \cdot 10^{-1}$
<b>775 °C</b>	$6.48 \cdot 10^{-5}$	$7.29 \cdot 10^{-3}$	$2.83 \cdot 10^{-1}$	$5.19 \cdot 10^{-1}$	$1.90 \cdot 10^{-1}$
<b>750 °C</b>	$4.0 \cdot 10^{-5}$	$4.80 \cdot 10^{-3}$	$1.68 \cdot 10^{-1}$	$6.28 \cdot 10^{-1}$	$2.0 \cdot 10^{-1}$
<b>725 °C</b>	$2.39 \cdot 10^{-5}$	$2.39 \cdot 10^{-3}$	$1.28 \cdot 10^{-1}$	$6.67 \cdot 10^{-1}$	$2.032 \cdot 10^{-1}$
<b>700 °C</b>	$7.93 \cdot 10^{-6}$	$1.59 \cdot 10^{-3}$	$7.93 \cdot 10^{-2}$	$7.12 \cdot 10^{-1}$	$2.07 \cdot 10^{-1}$

Table 10. Temperature distribution of the syngas OK800 and relative species quantities between 800 °C and 700 °C

	$X_{0,CH_4}$	$X_{0,H_2}$	$X_{0,CO}$	$X_{0,CO_2}$	$X_{0,H_2O}$
<b>800 °C</b>	$8.168 \cdot 10^{-5}$	$9.72 \cdot 10^{-3}$	$3.66 \cdot 10^{-1}$	$4.41 \cdot 10^{-1}$	$1.832 \cdot 10^{-1}$
<b>762.5 °C</b>	$5.225 \cdot 10^{-5}$	$5.63 \cdot 10^{-3}$	$2.09 \cdot 10^{-1}$	$5.89 \cdot 10^{-1}$	$1.96 \cdot 10^{-1}$
<b>725 °C</b>	$2.39 \cdot 10^{-5}$	$2.39 \cdot 10^{-3}$	$1.28 \cdot 10^{-1}$	$6.67 \cdot 10^{-1}$	$2.032 \cdot 10^{-1}$
<b>687.5 °C</b>	$5.94 \cdot 10^{-6}$	$7.92 \cdot 10^{-4}$	$7.13 \cdot 10^{-2}$	$7.2 \cdot 10^{-1}$	$2.08 \cdot 10^{-1}$
<b>650 °C</b>	$3.95 \cdot 10^{-6}$	$3.95 \cdot 10^{-4}$	$3.16 \cdot 10^{-2}$	$7.57 \cdot 10^{-1}$	$2.11 \cdot 10^{-1}$

Table 11. Temperature distribution of the syngas OK800 and relative species quantities between 800 °C and 650 °C

For the evaluation of the power output distribution it has been obtained the relative value simulating cell by cell and extracting the value of the produced power, because the cells in the stack are independent of each other. The results of the electrical power provided by the two configuration are reported in the graphs in Figures 28 and 29. As it can be noticed, in the air cooling system the power output is always higher in the 800 – 750 °C distribution, instead in the other two distribution the behaviour is quite similar in the cells that aren't near the inlet of biomass. The other two cells (position 0 and 0.05 m) work well with the air cooling system.

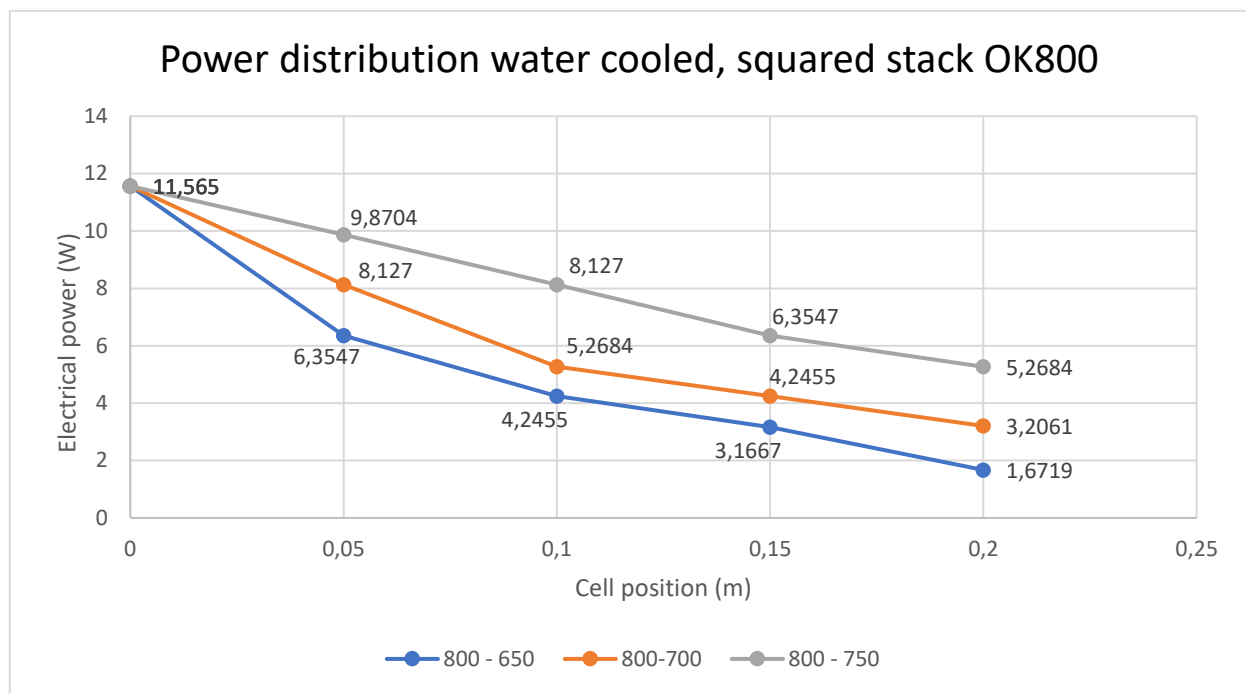


Figure 28. Electrical power developed by every cell in the three temperature distribution with water cooling system

So, the stack cooled by water is able to produce 206 W in the distribution 800 °C-750 °C, 162 W in the intermediate distribution and 135 W in the widest one. These values are obtained putting in series the cells on the same column. Therefore, the target of 200 W is reached only if the distribution inside the stack will be of the type 800 °C -750 °C, with the other two distribution the project goal is not satisfied also if one puts 30 cells inside the stack, because the electrical power will be 194 W in the intermediate temperature distribution and 162 W in the wider distribution.

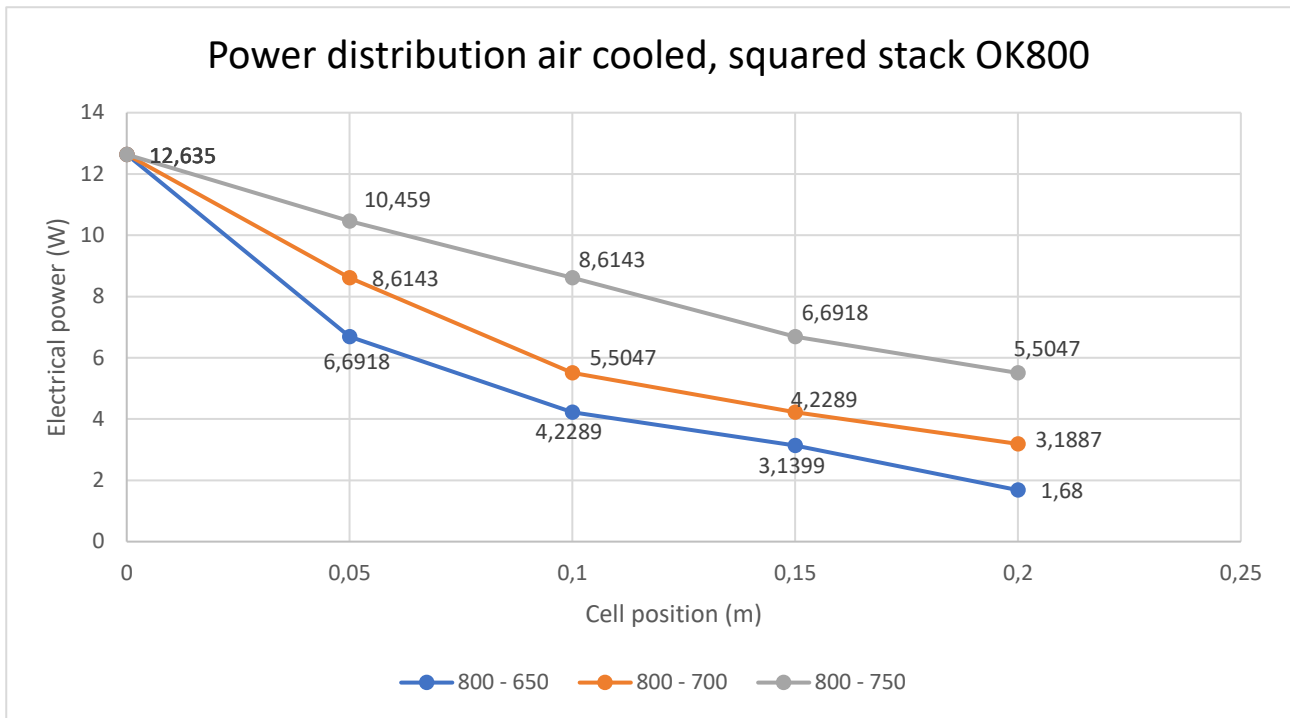


Figure 29. Electrical power developed by every cell in the three temperature distribution with air cooling system

Little higher results has been recorded with the air cooling system: the squared stack in the narrowest distribution produced 219 W of electrical power and in the other two distribution is able to provide 171 W and 142 W. The 800 – 650 °C distribution don't reach the target of the project also if one puts 30 cells inside the stack, instead the intermediate distribution is able to provide a little higher power than the 200 W, precisely 205 W of power production.

So, the resulting increment of power adopting the air cooling system amounts to 13 W.

Instead, the effective distribution temperature, with an inlet syngas distribution of 50 °C, inside the stack, in the case of heat is removed by water, is always lower than the air cooling system. In fact, if it is considered the average temperatures of syngas, cell and air, results that there is a difference of almost 2 °C in the distribution of the syngas average temperature, 4°C in the distribution of cell average temperature and almost 33 °C in the distribution of cathodic air temperature. The highest difference can be noticed in the cathodic air temperature because the water cooling system can reach to subtract more heat to the stack due to the fluid temperature is low.

	<i>Average temperature with water cooling</i>	<i>Average temperature with air cooling</i>
$\Delta T_{syngas}$	75.98	77.75
$\Delta T_{cell}$	98.31	102.39
$\Delta T_{air}$	96.72	129.6

Table 12. Effective distribution inside the stack powered by biomass OK800

and, as it can be noticed by the graphs in Figure 30, the trend of the effective temperatures of syngas continues to follow a linear trend in all the cooling system.

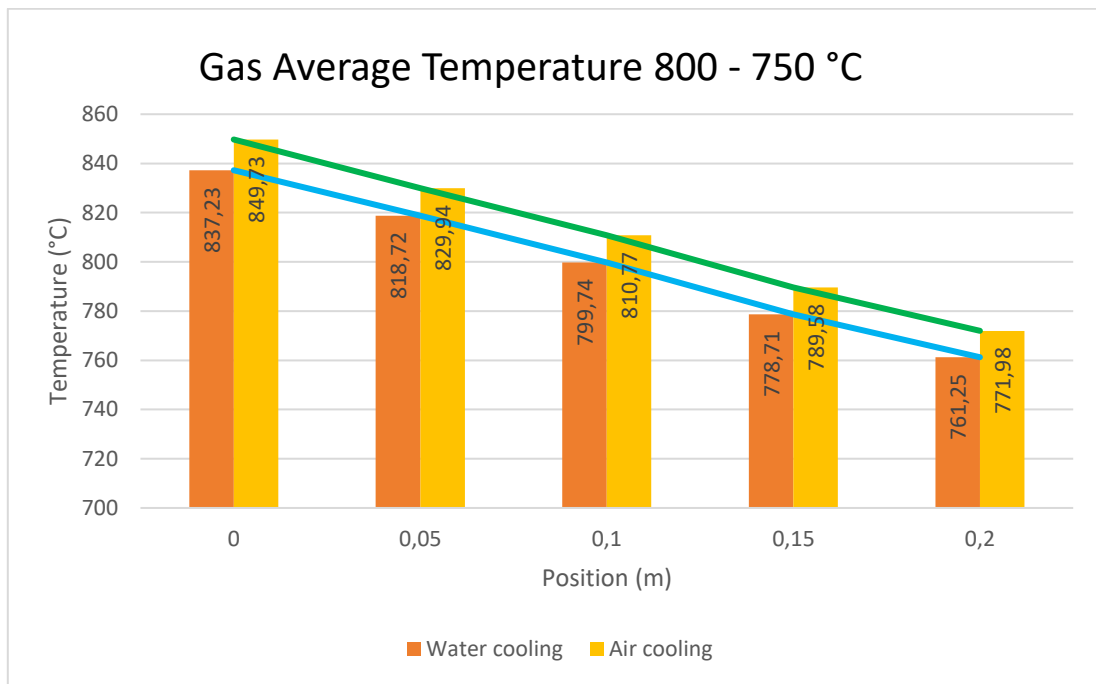


Figure 30. Trend of the average temperatures of syngas OK800 for the two cooling system

#### 5.4.1.2 OK500: air cooling system

In the end, it has been decided to re-compute the simulations of the distributions with the pre-treated biomass at 500 °C because in the first periodic report of the DB-SOFC project[24] is written that is the most reactive biomass of all those analyzed. Initially, it is necessary to extract the input values for each species of the syngas at every temperature of the distributions following the passages done for the evaluation of them for the biomass OK800. The cooling system adopted for these evaluation is

the one with air, as cooling fluid, at 650 °C, because it is revealed the better way to harness electrically the system. In the Tables 13, 14 and 15 are reported the molar fraction of each syngas constituent.

	$X_{0,CH4}$	$X_{0,H2}$	$X_{0,CO}$	$X_{0,CO2}$	$X_{0,H2O}$
800 °C	$9.806 \cdot 10^{-5}$	$4.34 \cdot 10^{-3}$	$3.84 \cdot 10^{-1}$	$4.29 \cdot 10^{-1}$	$1.829 \cdot 10^{-1}$
787.5 °C	$1.06 \cdot 10^{-4}$	$4.48 \cdot 10^{-3}$	$3.42 \cdot 10^{-1}$	$4.68 \cdot 10^{-1}$	$1.861 \cdot 10^{-1}$
775 °C	$1.06 \cdot 10^{-4}$	$4.87 \cdot 10^{-3}$	$3.08 \cdot 10^{-1}$	$4.98 \cdot 10^{-1}$	$1.89 \cdot 10^{-1}$
762.5 °C	$1.12 \cdot 10^{-4}$	$4.84 \cdot 10^{-3}$	$2.42 \cdot 10^{-1}$	$5.59 \cdot 10^{-1}$	$1.94 \cdot 10^{-1}$
750 °C	$1.21 \cdot 10^{-4}$	$5.23 \cdot 10^{-3}$	$2.25 \cdot 10^{-1}$	$5.74 \cdot 10^{-1}$	$1.95 \cdot 10^{-1}$

Table 13. Temperature distribution of the syngas OK500 and relative species quantities between 800 °C and 750 °C

	$X_{0,CH4}$	$X_{0,H2}$	$X_{0,CO}$	$X_{0,CO2}$	$X_{0,H2O}$
800 °C	$9.806 \cdot 10^{-5}$	$4.34 \cdot 10^{-3}$	$3.84 \cdot 10^{-1}$	$4.29 \cdot 10^{-1}$	$1.829 \cdot 10^{-1}$
775 °C	$1.06 \cdot 10^{-4}$	$4.87 \cdot 10^{-3}$	$3.08 \cdot 10^{-1}$	$4.98 \cdot 10^{-1}$	$1.89 \cdot 10^{-1}$
750 °C	$1.21 \cdot 10^{-4}$	$5.23 \cdot 10^{-3}$	$2.25 \cdot 10^{-1}$	$5.74 \cdot 10^{-1}$	$1.95 \cdot 10^{-1}$
725 °C	$1.60 \cdot 10^{-4}$	$5.60 \cdot 10^{-3}$	$1.52 \cdot 10^{-1}$	$6.42 \cdot 10^{-1}$	$2.01 \cdot 10^{-1}$
700 °C	$2.79 \cdot 10^{-4}$	$5.97 \cdot 10^{-3}$	$1.12 \cdot 10^{-1}$	$6.79 \cdot 10^{-1}$	$2.04 \cdot 10^{-1}$

Table 14. Temperature distribution of the syngas OK500 and relative species quantities between 800 °C and 700 °C

	$X_{0,CH4}$	$X_{0,H2}$	$X_{0,CO}$	$X_{0,CO2}$	$X_{0,H2O}$
800 °C	$9.806 \cdot 10^{-5}$	$4.34 \cdot 10^{-3}$	$3.84 \cdot 10^{-1}$	$4.29 \cdot 10^{-1}$	$1.829 \cdot 10^{-1}$
762.5 °C	$1.12 \cdot 10^{-4}$	$4.84 \cdot 10^{-3}$	$2.42 \cdot 10^{-1}$	$5.59 \cdot 10^{-1}$	$1.94 \cdot 10^{-1}$
725 °C	$1.60 \cdot 10^{-4}$	$5.60 \cdot 10^{-3}$	$1.52 \cdot 10^{-1}$	$6.42 \cdot 10^{-1}$	$2.01 \cdot 10^{-1}$
687.5 °C	$3.34 \cdot 10^{-4}$	$6.36 \cdot 10^{-3}$	$9.54 \cdot 10^{-2}$	$6.93 \cdot 10^{-1}$	$2.05 \cdot 10^{-1}$
650 °C	$5.55 \cdot 10^{-4}$	$7.53 \cdot 10^{-3}$	$6.34 \cdot 10^{-2}$	$7.21 \cdot 10^{-1}$	$2.07 \cdot 10^{-1}$

Table 15. Temperature distribution of the syngas OK500 and relative species quantities between 800 °C and 650 °C

Now, in the simulations are recorded the power distribution of the type reported in Figure 31, so the squared stack is able to provide 225 W of electrical power, if on it is present a temperature distribution between 800 °C and 750 °C, connecting 5 cells of the same column. This value is only 6 W higher than the correlative configuration with biomass OK800, therefore, even if the power is lower, the best solution is the squared stack powered by the biomass OK800 with a temperature distribution between 800°C and 750 °C because for the one with biomass OK500 it is necessary to increase the temperature of the pre-treated biomass in an inert atmosphere of 300 °C. This procedure could be done with an electrical resistance or with the combustion of a fraction of syngas developed by the gasification in a pre-heating chamber.

The other two distribution aren't able to reach the prefixed goal, since they develop powers of 173 W and 139 W.

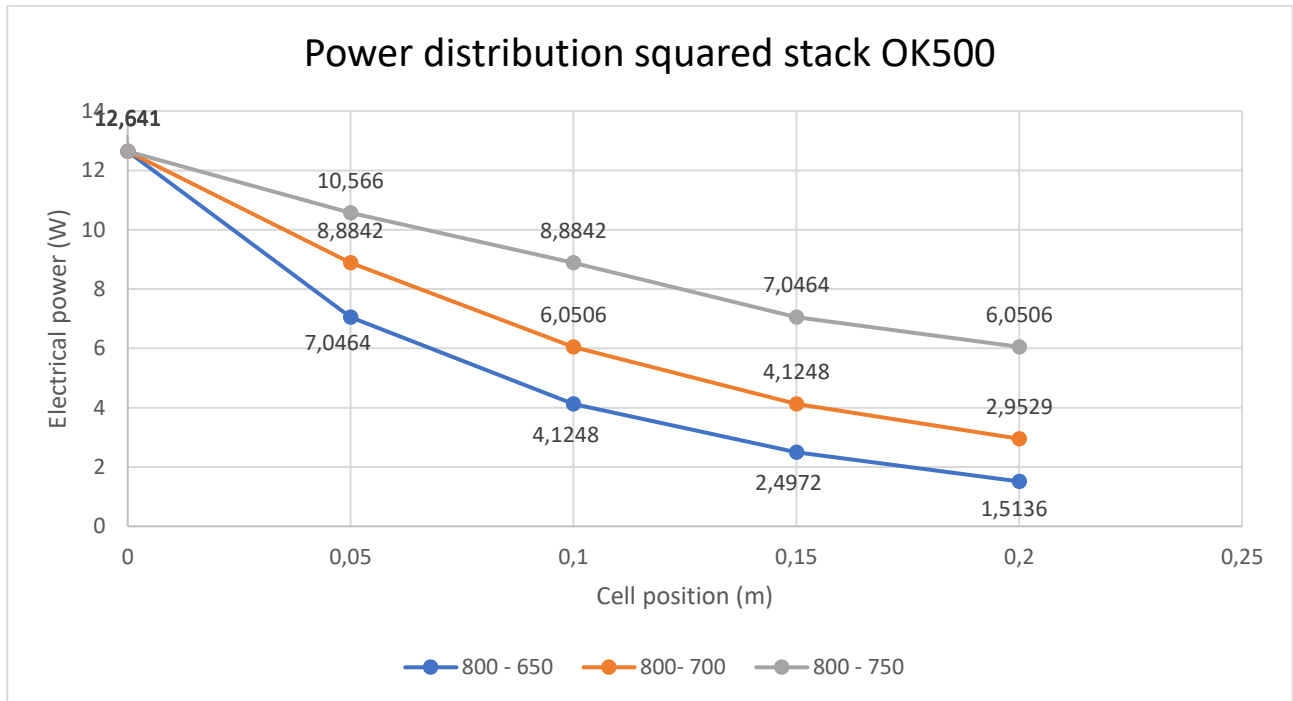


Figure 31. Power distribution inside the squared stack of a row of cells alimeted by syngas derived by the gasification of the biomass OK500

For what concern the effective temperature distribution for the feasible solution, now it can be found the values reported in the Table 16.

*Average temperature with air cooling*

$\Delta T_{syngas}$	73.85
$\Delta T_{cell}$	94.82
$\Delta T_{air}$	92.24

Table 16. Effective distribution for the stack powered by biomass OK500

All the three temperature differences between the first cell (near the inlet of biomass) and the last cell of the row are lower than the case of stack powered by biomass OK800 and cooled by air, even if the temperature in the three domain of the first cell is almost equal, because the syngas produced from the gasification of the biomass OK500 has an higher amount of CO and H<sub>2</sub> in the syngas at the final temperature of the distribution.

## 5.4.2 Circular stack

### 5.4.2.1 OK800 circular: water and air cooling system

For the evaluation of the power generated by the circular configuration of the stack, it has re-built the geometry of it, as described in the paragraph 3.2. Then, it has been assigned at the five cells along the x-axis the same distributions of temperature of the squared stack and for the cell in between it has been used a proportion to find the temperature of every cell and putting it on a linear interpolation to calculate the power provided by each cell.

The resulting power outputs for the cells in the various position inside the stacks are the following and, in this stack, the nearest cell to the inlet of biomass is represented by the position -0.12 m.

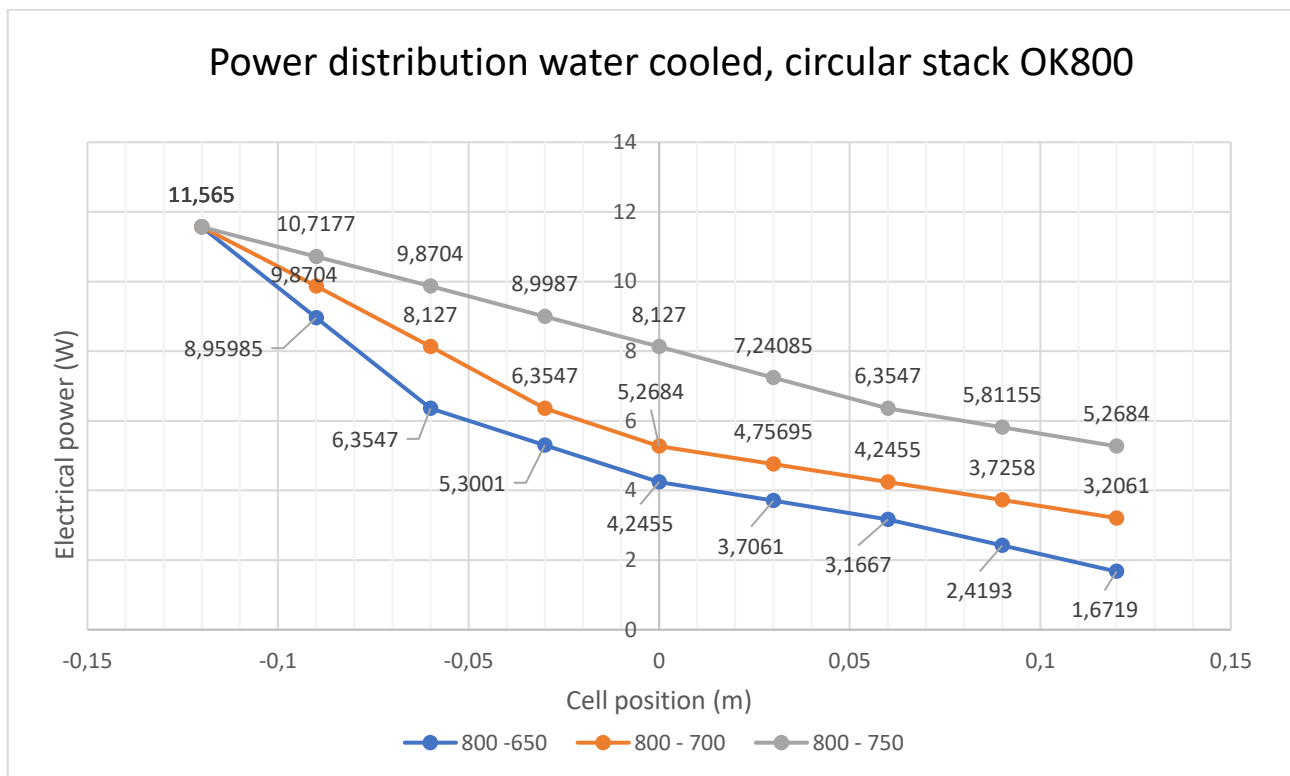


Figure 32. Distribution of power provided by the cell in every position inside the stack cooled by water and powered by OK 800

Also in this case the highest difference between the two cooling system can be found near the injection of the biomass in the stack.

Moreover, to calculate the entire power of the stack it has supposed to connect in series 5 cells with similar provided current, so the decision has been:

- connect the 5 cells in position 0 m in series
- connect 4 cells in position -0.03 m with 1 cells in position -0.06 m and, simmetrically, the corresponsive cells on the right of the stack
- connect the last 10 cells, five by five, on the right and on the left of the stack

The resulting powers for the distributions are:

- in the 800 -750 °C, 193 W for the water cooling system and 204 W for the air cooling system
- in the 800 -700 °C, 136 W for the water cooling system and 141 W for the air cooling system
- in the 800 -650 °C, 104 W for the water cooling system and 106 W for the air cooling system

As it can be noticed, the power reaches the target of the project only in one cases, but the voltage of every five cells connected in series could be lower than 3.5 V, that is the value used to calculate the powers. The value of current used is the one of the weakest cell of the series.

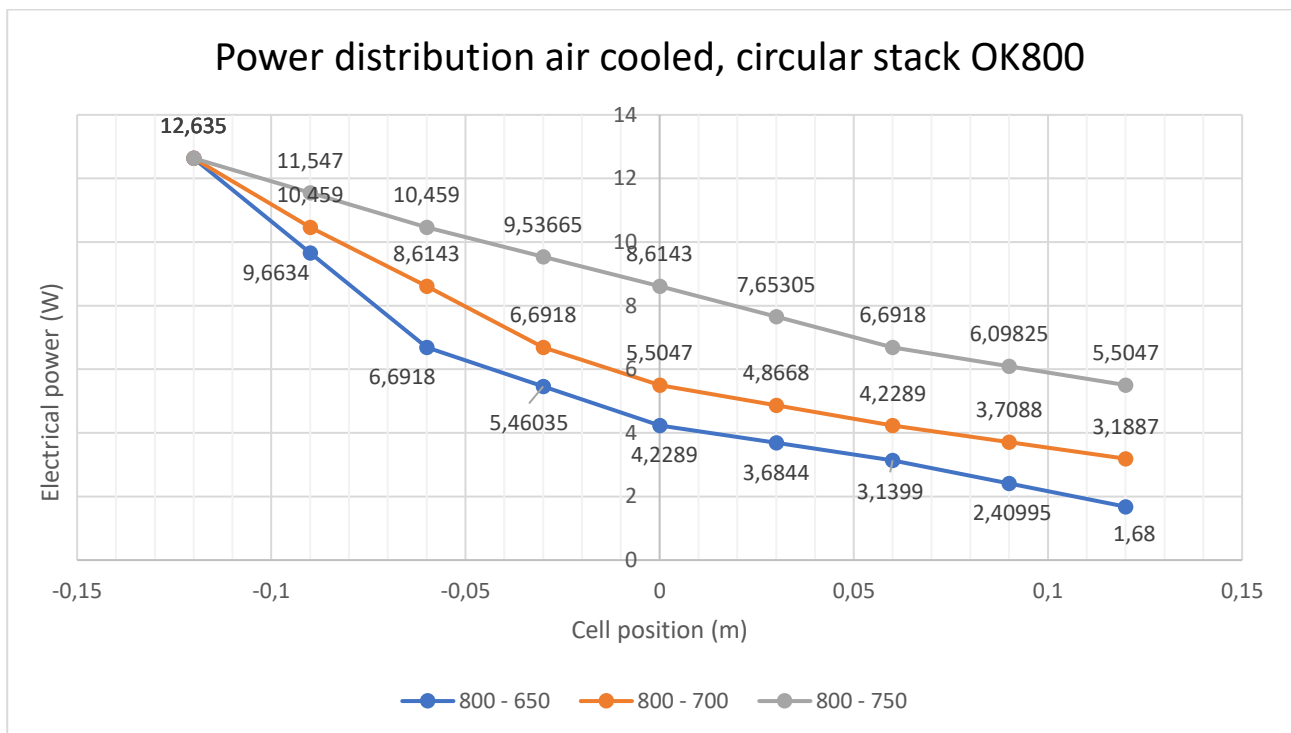


Figure 33. Distribution of power provided by cells in every position inside the stack cooled by air and powered by OK 800

### 5.4.2.2 OK500 circular: air cooling system

For the circular stack, alimeted by biomass pre-treated at 500 °C, the evaluation of the power of the cells is conducted in the same way of the OK800 biomass case. The resulting power outputs are, now, 211 W for the smallest  $\Delta T$  distribution, 147 W for the intermediate one and 104 W for the largest temperature distribution.

Also in this case the values of electrical power are obtained multiplying the total voltage of 5 cells in series (3.5 V) with the value of current produced by the weak cell of the series. This is an approximation, so the current can affect the voltage of the stronger cells decreasing it and, as a consequence, the total power that the stack is able to produce.

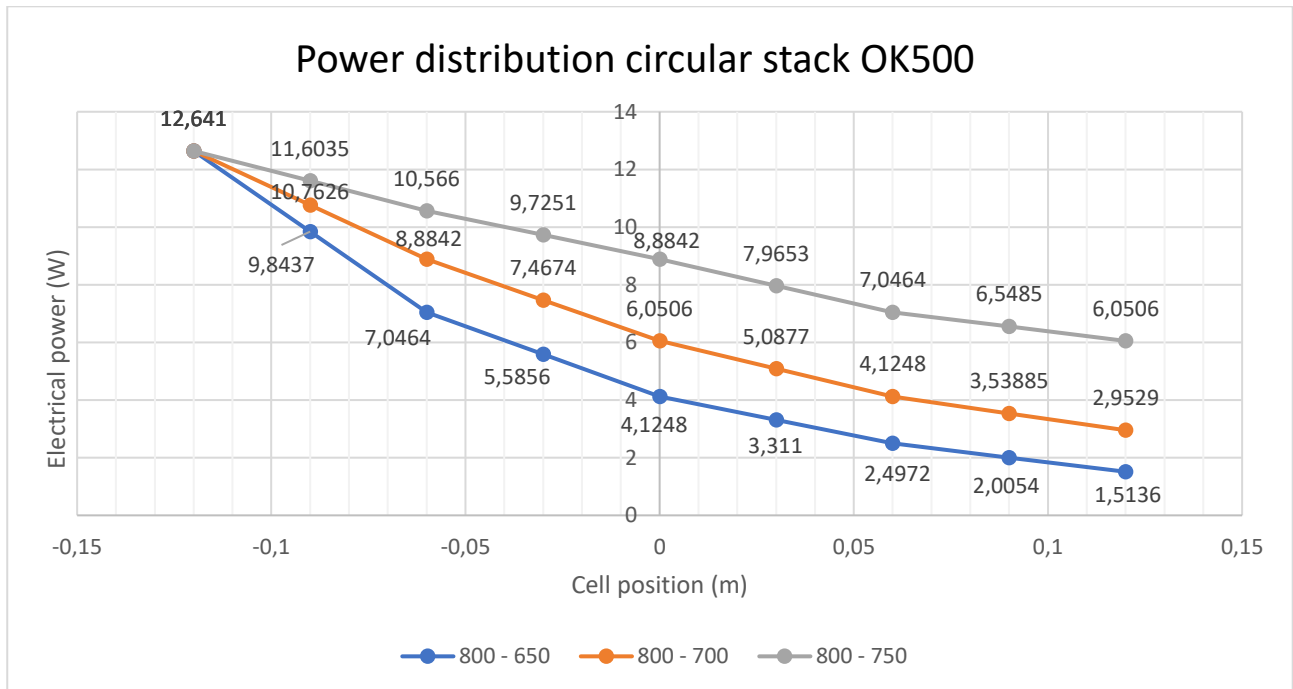


Figure 34. Power distribution inside the circular stack of a row of cells alimeted by syngas derived by the gasification of the biomass OK500

## 6 Conclusions

In conclusion, from the analysis of the different configurations comes out that the best solution in terms of extracted power will be the squared stack powered by the biomass pre-treated at 500 °C with its 225 W of electrical power developed considering a temperature distribution along the stack between 800°C and 750°C. However, with the pre-treated biomass OK500 a pre-heating chamber will have to be thought to heat up the solid fuel in an inert atmosphere to avoid the gasification on it and it could be heated up burning a part of the syngas that will be recirculated at the exiting from the stack, or with an electrical resistance. The other biomass, OK800, could provide only 6 W less than this, deleting the pre-heating problems, in the squared stack cooled by air.

More in general, it results that the circular configurations provide less power than the correspondent squared systems because this type of stack suffers the connection in series of cells that gives different current outputs, limiting the total current inside the series of cells to the lowest value.

From a thermal point of view, the cells are subjected to high temperatures, specially, on the lower part of the stack where the cooling systems don't reach to subtract heat in an efficient way, but the maximum values of them are lower than the maximum working temperature of SOFCs, that is near 1000 °C. The high temperatures could be an advantage for the matching with the endothermic gasification process of the biomass that in reality covers a part of the bottom of cells. Instead, the minimum values of temperature recorded in the water cooling system are dangerous for the integrity of the cells. Moreover, the temperature distributions will have to be verified with studies on the biomass gasification, because in this work are supposed linearly decreasing between the inlet of the biomass and the outlet of the exhaust syngas.

Another important aspect that will have to be confirmed is the geometry of the cooling system to confirm the validity of the assumption done for the heat transfer coefficients in this thesis, then also the inlet syngas and air velocities will be validated.

At the end, to make as real as possible the system, the carbon deposition phenomena, that could be arise during the operation in real conditions, and the obstruction due to the solid biomass would be studied. Also a better system to collect the current and, so, to manage the electrons provided by each cell could be developed.

All the validation will be conducted in future works, don't have to reduce the optimistic results of this thesis more than 11 % in the case of the biomass OK500, or 8% in the case of the biomass OK800 inside the squared stack cooled by air, to reach the prefixed goal of 200 W for the entire stack.



## 7 Bibliography

- [1] A. Molino, S. Chianese, and D. Musmarra, “Biomass gasification technology: The state of the art overview,” *J. Energy Chem.*, vol. 25, no. 1, pp. 10–25, 2016.
- [2] C. Parisius, “DB-SOFC DB-SOFC ERANETMED2-72-246,” pp. 1–45, 2020.
- [3] M. E. A. Jones Alami, “Report on the availability of Biomass Sources in Morocco : vineyards and olive groves,” no. December 2017, pp. 1–16, 2018.
- [4] “DRAFT - Biomass Availability.” .
- [5] M. S. Jesus, A. Romani, Z. Genisheva, J. A. Teixeira, and L. Domingues, “Integral valorization of vine pruning residue by sequential autohydrolysis stages,” *J. Clean. Prod.*, vol. 168, pp. 74–86, 2017.
- [6] R. Guidelli *et al.*, “Defining the transfer coefficient in electrochemistry: An assessment (IUPAC Technical Report),” *Pure Appl. Chem.*, vol. 86, no. 2, pp. 245–258, 2014.
- [7] B. A. Haberman and J. B. Young, “Three-dimensional simulation of chemically reacting gas flows in the porous support structure of an integrated-planar solid oxide fuel cell,” *Int. J. Heat Mass Transf.*, vol. 47, no. 17–18, pp. 3617–3629, 2004.
- [8] C. Guizani, “Effects of CO<sub>2</sub> on the biomass pyro-gasification in high heating rate and low heating rate conditions,” p. 189, 2014.
- [9] K. SATO, M. NAITO, and H. ABE, “Electrochemical and mechanical properties of solid oxide fuel cell Ni/YSZ anode fabricated from NiO/YSZ composite powder,” *J. Ceram. Soc. Japan*, vol. 119, no. 1395, pp. 876–883, 2011.
- [10] D. Cui, L. Liu, Y. Dong, and M. Cheng, “Comparison of different current collecting modes of anode supported micro-tubular SOFC through mathematical modeling,” *J. Power Sources*, vol. 174, no. 1, pp. 246–254, 2007.
- [11] S. P. Muhoza *et al.*, “High Surface Area SOFC Electrode Materials Prepared at Traditional Sintering Temperatures,” *J. Electrochem. Soc.*, vol. 165, no. 2, pp. F46–F54, 2018.
- [12] M. Ni, “Modeling of SOFC running on partially pre-reformed gas mixture,” *Int. J. Hydrogen Energy*, vol. 37, no. 2, pp. 1731–1745, 2012.
- [13] M. Santarelli, P. Leone, M. Cali, and G. Orsello, “Experimental evaluation of the sensitivity

- to fuel utilization and air management on a 100 kW SOFC system,” *J. Power Sources*, vol. 171, no. 1, pp. 155–168, 2007.
- [14] S. P. Jiang, *Development of lanthanum strontium manganite perovskite cathode materials of solid oxide fuel cells: A review*, vol. 43, no. 21. 2008.
- [15] R. C. Buchanan and S. Pope, “Optical and Electrical Properties of Yttria Stabilized Zirconia Crystals.”
- [16] M. Andersson, J. Yuan, and B. Sundén, “SOFC modeling considering electrochemical reactions at the active three phase boundaries,” *Int. J. Heat Mass Transf.*, vol. 55, no. 4, pp. 773–788, 2012.
- [17] V. Somano, “CFD model for tubular SOFC fed directly by biomass,” 2019.
- [18] M. Ni, “2D heat and mass transfer modeling of methane steam reforming for hydrogen production in a compact reformer,” *Energy Convers. Manag.*, vol. 65, no. 852, pp. 155–163, 2013.
- [19] T. X. Ho, P. Kosinski, A. C. Hoffmann, and A. Vik, “Numerical modeling of solid oxide fuel cells,” *Chem. Eng. Sci.*, vol. 63, no. 21, pp. 5356–5365, 2008.
- [20] M. Ceriani, “Analisi di modello di SOFC alimentate con gas di sintesi,” p. 1633, 2015.
- [21] I. Gholaminezhad, M. H. Paydar, K. Jafarpur, and S. Paydar, “Multi-scale mathematical modeling of methane-fueled SOFCs: Predicting limiting current density using a modified Fick’s model,” *Energy Convers. Manag.*, vol. 148, pp. 222–237, 2017.
- [22] R. C. Reid, T. K. Sherwood, and R. E. Street, *The Properties of Gases and Liquids*, vol. 12, no. 4. 2009.
- [23] W. Lehnert, J. Meusinger, and F. Thom, “Modelling of gas transport phenomena in SOFC anodes,” *J. Power Sources*, vol. 87, no. 1, pp. 57–63, 2000.
- [24] P. Id, “ERANETMED First Joint Call ( 1 st JC ) Periodic Activity Report ( Month 1 ~ 6 ),” pp. 1–56, 2003.